2(mx)

University of Arizona Grant NGR-03-002-275
Dudley Observatory Grant NGR-33-011-033
Univ. California(Los Angeles) NGR-05-007-226

FINAL TECHNICAL REPORT

OUTER PLANET GRAND TOUR MISSIONS PHOTOMETRY/POLARIMETRY EXPERIMENT CRITICAL COMPONENTS STUDY

For - The Photometry/Polarimetry Experiment Team
Contract W26157, Issued by
The Lunar and Planetary Laboratory,
University of Arizona
Tucson, Arizona

Also Jointly supported by NASA under the above grants

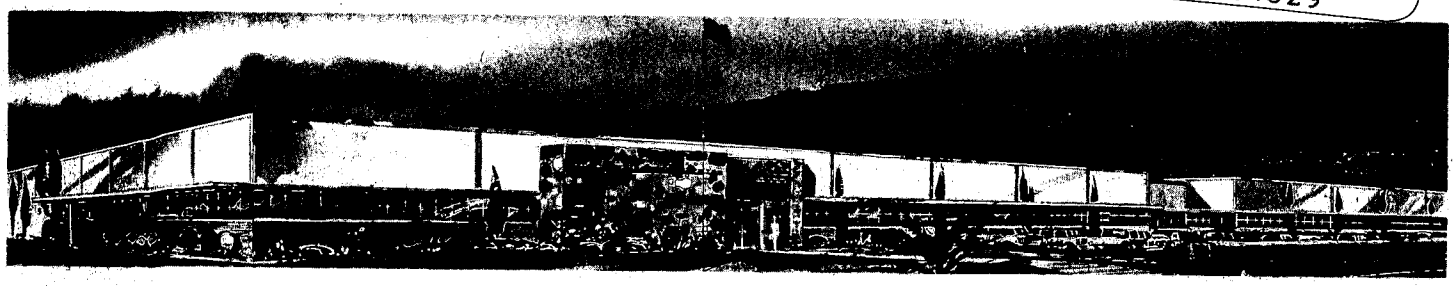

SANTA BARBARA RESEARCH CENTER
A Subsidiary of Hughes Aircraft Company
SBRC

U.S. DEPARTMENT OF COMMERCE
National Technical Information Service
5285 Port Royal Road
Springfield, Virginia 22151

Date: June 25, 1973

Reply to Attn of: 954.01

Subject: NASA Document Discrepancy Report 73-247

To: Mr. E. E. Baker
Deputy General Manager
Informatics TISCO
P. O. Box 33
College Park, Maryland 20740

Re: N 73-19427

☒ 1. Page(s) are missing from microfiche and paper copy. Please provide a complete copy. Page 7-2. OK

☒ 2. Portions of this document are illegible when reproduced. Please provide a reproducible copy. Page 4-2.

☐ 3. A microfiche reproduction is not legible. The case file was not received. Please provide at least an acceptable microfiche.

☐ 4. Incorrectly priced at _____. It should be _____ for _____ pages. However, price will remain as announced in STAR.

☒ 5. Case file returned herewith. When correction has been made please return to NTIS or if corrections cannot be made note NASA records that the case file was returned.

☐ 6. Other:

C/S # 74-2920

14 Nov 74

C/S to BA/MA/e (Auth. - Baba, NASA)
Taye

11/14/74 Pam Little

November 8, 1974

Forwarded herewith is a corrected paper copy and microfiche copy of N73-19427 for your permanent retention. Contained in these items are the best available copies of pages 7-2 and 4-2.

Sincerely,

Barbara Reed

E. E. Baker
Deputy General Manager

Phone: 703 -321-8517

Response

Before After
___ Issue Ch. of Status ___
Code XN/XN/Y Code
___ Comp. Ser.-No Act. ___
___ Delay Ch. OF Status ___
X Post(ed) on Form 107 ___

FC/BR/djr

PLEASE ATTACH COPY OF THIS LETTER WITH YOUR RESPONSE

SANTA BARBARA RESEARCH CENTER

A Subsidiary of Hughes Aircraft Company

75 COROMAR DRIVE • GOLETA, CALIFORNIA

FINAL TECHNICAL REPORT

OUTER PLANET GRAND TOUR MISSIONS

PHOTOMETRY/POLARIMETRY EXPERIMENT

CRITICAL COMPONENTS STUDY

for

The Photometry/Polarimetry Experiment Team
Contract W26157, Issued by
The Lunar and Planetary Laboratory,
University of Arizona
Tucson, Arizona

Revision 1

30 May 1972

Prepared by S. F. Pellicori
S. F. Pellicori
Member of Technical Staff

Approved by R. F. Hummer
R. F. Hummer, Manager
Electro-Optical
Instrumentation

Prepared by E. E. Russell
E. E. Russell
Member of Technical Staff

Prepared by L. A. Watts
L. A. Watts
Member of Technical Staff

CONTENTS

ILLUSTRATIONS

ILLUSTRATIONS (Cont)

ILLUSTRATIONS (Cont)

TABLES

Section 1
INTRODUCTION

The purpose of this Final Technical Report is to present the results of a study effort performed in support of a NASA-formed Science Team for Photopolarimetry. The study was sponsored by the Lunar and Planetary Laboratory of the University of Arizona as part of an overall contract funded by NASA under the Mission Definition Phase of the Outer Planets Grand Tour (OPGT) Program (later changed to Mariner Jupiter/Saturn Program). Ultimately, the science team is charged with defining an instrument/experiment capable of performing photometry and polarimetry investigations of the outer planets aboard an outer-planets spacecraft. This report covers a part of that effort, namely, the tasks which were assigned to SBRC.

Work performed during this effort was limited to two primary areas of technical concern: optical design optimization, and sensor selection. These were identified by SBRC as areas which might require significant improvement over previous instrument design technology in order for an instrument to function under the rigorous requirements of these extended outer planet missions. (Other technical problem areas were assigned to various other organizations by the scientific team.)

An optical system concept was established, and various of the system components were evaluated through experimental test sequences. This optical system, herein recommended by SBRC for the specified multipurpose photometry/polarimetry/zodiacal light experiments, represents the culmination of many trade-off studies, concept iteration exercises, and component evaluations. This design, in addition to being adequate to meet or exceed operational requirements, incorporates some new and sophisticated techniques, is physically simple, and may be made lightweight, rugged, and stable. It is fully described in a subsequent section.

In the second area of study, photodetectors were investigated for their applicability in meeting OPGT requirements as constrained by the photometry/polarimetry team directives. The most promising (gallium arsenide PMT) was further experimentally tested to ascertain its behavior with respect to anticipated environmental conditions. Results of this testing and a summary of the preceding trade-off study effort are presented in the following text.

Section 2
BACKGROUND

SBRC became involved in the OPGT mission definition as a result of previous experience gained in developing the Pioneer F/G Imaging Photopolarimeter instrument (IPP). Originally, the intent was to use as much as possible of the existing IPP design, making only those changes necessary to satisfy the more severe multiplanet mission requirements of long-life, added redundancy, etc. However, as additional functional requirements were found necessary to accommodate mission scientific objectives, an iterative process began to evolve an instrument far too large and heavy for practical consideration.

A new instrument configuration, described in the following section, was conceived after a series of discussions with the science team. Although this concept may be mechanized in a variety of ways, the one chosen for presentation here represents a compromise which minimizes size, weight, telemetry bandwidth, and cost. It retains polarimetric precision by measuring orthogonal components simultaneously, but sacrifices utility in requiring that polarimetric measurements in the various spectral bands be made sequentially.

An optical component study effort was conducted nearly as originally projected. During the course of the detector study, however, emphasis was redirected from a detector selection activity to primarily a test and evaluation activity. This change in emphasis was made when it became evident that the newly developed gallium arsenide (GaAs) type photomultiplier tubes offered the possibility that a single detector could cover the entire spectral range of interest with sufficient dynamic range to perform precision planetary photometry while yet providing adequate zodiacal light measurement. Use of a pair of these PM tubes could contribute to a significant weight reduction over the multidetector configuration previously proposed.

Because the GaAs device is relatively new, little historical data were available related to short-term operation under environmental conditions, or to long-term stability characteristics. Therefore, a tube was procured and evaluated in terms of long-term stability, gain characteristics, angle of incidence sensitivity, cathode uniformity, and radiation resistance.

Section 3
GENERAL SYSTEM CONSIDERATIONS

SCOPE

Although systems analysis was not assigned to SBRC as a part of this study — this was retained as a science committee function — it was obvious to us that some SBRC effort was essential in this area. Since the University of Colorado (LASP) was assigned the electronics and mechanics portions of the study, we at SBRC did not expend effort in these areas during the study. Specific contributions in these two areas were made during informal meetings and science committee sessions where experience gleaned from the twenty-six SBRC sensors of different types launched and successfully operated in space was offered. We felt that the conceptual design was a key area, and this was given careful consideration during the study. In addition, early in the study, signal-to-noise (SNR) calculations were made to assist the science team in making trade-offs between various sensor parameters.

CONCEPTUAL DESIGN

A number of constraints and conditions lead to the selected design. These included: 1) the requirement to sense both planetary (three planet encounters assumed) and zodiacal light radiance levels with adequate SNRs; 2) the capability for both radiometric and polarimetric measurements over five specific spectral intervals from about 250 to 830 nm; 3) adequate inflight radiometric and polarimetric calibration; and 4) mission constraints including weight, power, reliability and the radiation environment, among others. The primary elements of the selected design are indicated in Figure 3-1.

Briefly, the photometer-polarimeter functions as follows. Flux from the scene is collected by the telescope and focused onto a field-defining aperture positioned at the focal plane. As indicated in Figure 3-1, it is anticipated that four field-defining apertures will provide the required versatility with

TOPS PHOTOPOLARIMETER

APERTURE ASSEMBLY	
Position	Aperture Characteristics
A	3° Circular Aperture
B	Radioisotope Phosphor Source for Sky Map Calibration
C	Diffuse Reflective Area for Inflight Calibration
D-F	Square and Slit Apertures Optimized for Selected Planetary Measurements

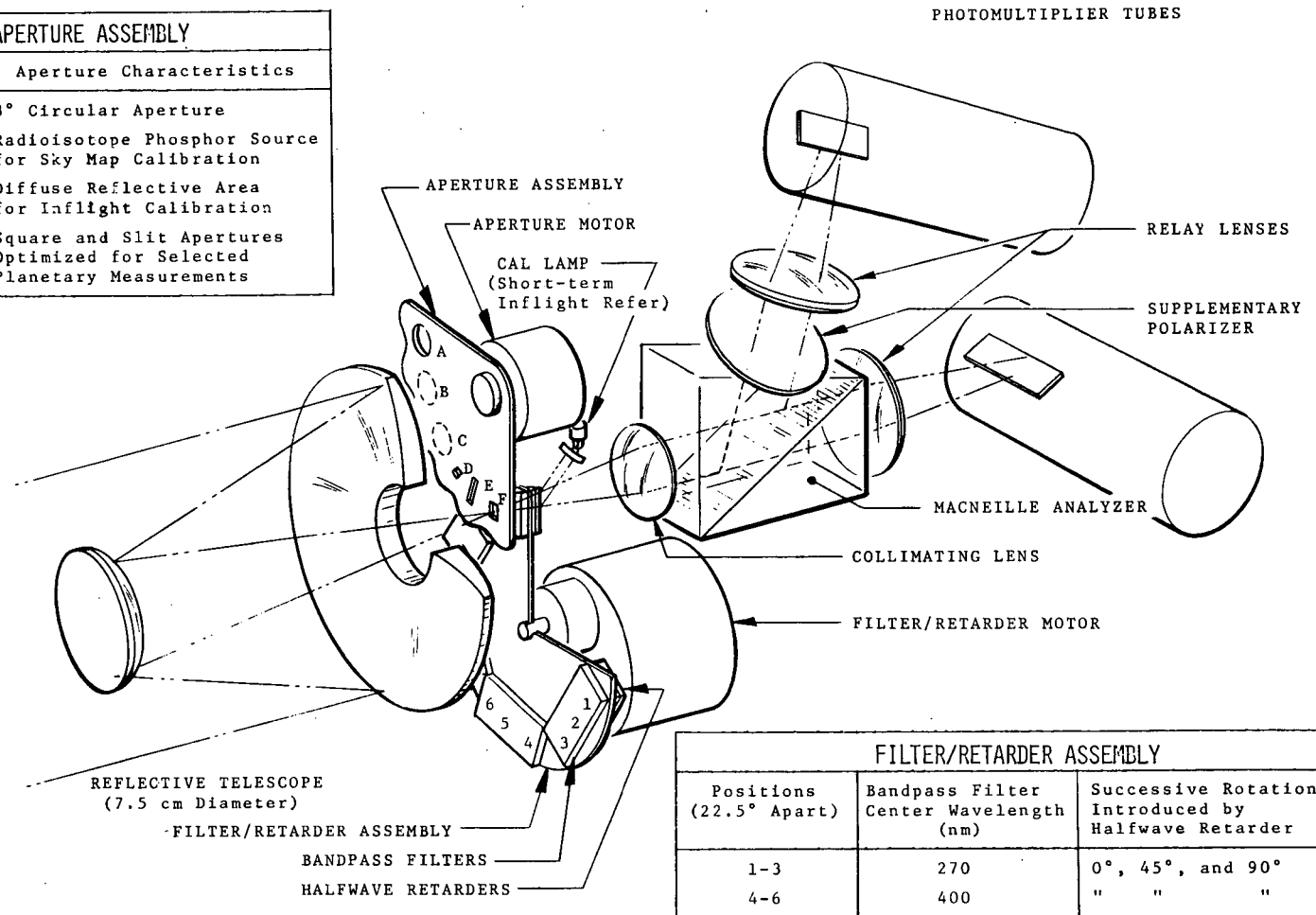

FILTER/RETARDER ASSEMBLY		
Positions (22.5° Apart)	Bandpass Filter Center Wavelength (nm)	Successive Rotations Introduced by Halfwave Retarder
1-3	270	0°, 45°, and 90°
4-6	400	" " "
7-9	540	" " "
10-12	727	" " "
13-15	820	" " "
16	Opaque Sector	Dark Current Reference

Figure 3-1. Schematic Representation of Two-Channel, Multiple Wavelength Photometer-Polarimeter

respect to varying scene radiance and desired spatial definition. The flux passed by the field stop is defined spectrally by one of five bandpass filters. The half-wave retardation plates adjacent to the filters serve to modify (rotate) the azimuth of linear polarization components in the scene flux. Three successive 22.5° physical rotations are used for each spectral band to produce 0°, 45° and 90° rotations of the linear polarization components with respect to a fixed direction. The MacNeille analyzer then separates the incident flux into two orthogonal linear polarization components. A supplementary polarizer in the reflected beam from the MacNeille analyzer serves to eliminate the residual polarization defect of the analyzer. Finally, the flux in each channel is detected by a PMT equipped with a GaAs photocathode that yields the desired extended red spectral response. Appropriate orientation of the photocathodes as shown in Figure 3-1 serves to optimize the responsivity for each channel. The individual components of the photometer-polarimeter will be described in more detail in the following sections.

A number of calibration devices are used to provide the inflight calibration of the photopolarimeter. A short-term radiometric reference can be obtained by using a lamp to illuminate the opaque sector of the filter/retarder assembly. With the possible exception of the 270-nm band, an appropriate reflective surface coupled with one or more filter layers can provide reasonable flux levels for each of the spectral channels. The use of the sun diminished by an attenuator and/or stars will provide additional means of calibration for the instrument. Such approaches were successfully used on the Pioneer F/G Imaging Photopolarimeter.

The opaque position also provides a dark reference position when the lamp is not lighted. The zodiacal light radiometric calibration can be provided by one (or more) radioisotope-activated phosphor sources mounted on the aperture assembly. The polarimetric calibration is obtained by the use of the three distinct position angles of the half-wave retarder mentioned above. Since the 0° and 90° rotations produced by the half-wave retarder interchange

the roles of the detectors, this provides the means for relating the polarimetric responsivity of the two channels.

SNR CALCULATIONS

Due to the extremely low radiance of the zodiacal light, it was obvious early in the study that a photoemissive type, e.g., photomultipliers or channeltrons, would be required within the practical mission constraints such as size and weight for the instrument. For a photoemissive-type detector where the noise is predominantly signal shot noise, the SNR, i.e., peak signal to rms noise, is given by

$$\text{SNR} = \frac{D}{d}\left[\frac{\Omega(1-\epsilon)\int H_{\lambda,\odot}\, R(\lambda)p(\lambda)T(\lambda)d\lambda}{8ke\Delta f_n}\right]^{\frac{1}{2}} \qquad (1)$$

where
- D = telescope aperture diameter (cm)
- d = sun-object distance in A. U.
- Ω = field-of-view solid angle (sr)
- ϵ = telescope obscuration factor
- $H_{\lambda,\odot}$ = spectral irradiance of sun at earth (watts cm^{-2} nm^{-1})
- $R(\lambda)$ = spectral responsivity of detector (amps/watt) at λ (nm)
- $p(\lambda)$ = spectral geometric albedo of planet
- $T(\lambda)$ = spectral transmittance of optics
- k = PMT noise factor
- e = electron charge = 1.6×10^{-19} (coulomb)
- Δf_n = effective noise bandwidth (Hz)

The exact signal processing method, i.e., signal integration, low-pass filtering, pulse counting, etc., has only a minor effect on the SNR. Other considerations such as the required dynamic range, maximum count rate, etc., are of greater importance in the choice of the signal processing method. With the use of signal integration, the effective noise bandwidth Δf_n is given by

$$\Delta f_n = 1/(2T)$$

where T is the integration time.

In Table 3-1 the SNR results for 0° phase angle are given for the five outer planets assuming a 7.5-cm telescope and 1-second integration time. Note that an 8-mr (assumed square) field-of-view (FOV) aperture was used for the three outermost planets and 2 mr for Jupiter and Saturn. The spectral geometric albedo values are from Harris. (The values for the UV band were extrapolated.)

At the bottom of Table 3-1, an estimate of the instrument performance in the low light level (zodiacal light) mode is included for the five spectral bands. For this mode, a circular 3° FOV (2.15×10^{-3} sr) and a 10-second integration time were assumed with other instrumental parameters being the same as for the planetary measurements. A scene radiance equivalent to 100 10th magnitude stars/deg^2 or 1.3×10^{-13} watt cm^{-2} sr^{-1} nm^{-1} at 530 nm was used.

Since the spectral distribution of the zodiacal light is very nearly that of the sun, the spectral radiance for these calculations was assumed to follow that of a 5800°K blackbody. The SNRs given in the table can be scaled according to equation (1) so long as the dark current (dark count rate) is small compared to the signal current (signal count rate). In this case, the signal shot noise greatly exceeds the dark noise component.

Table 3-1. Calculated OPGT Photometer-Polarimeter Performance

OPGT PHOTO POLARIMETER PERFORMANCE FOR JUPITER WITH OMEGA= 0.4000000E-05SR AND INTEGRATION TIME= 1.SEC

WAVELENGTH (NM)	DELTA WVL (NM)	DET. RESP. (A/W)	OPTICAL TRANS.	ALBEDO	SPECTRAL RAD. (W/(CM2-SR-NM))	I CATHODE (A)	COUNT RATE (C/S)	S/N RATIO
270.	50.	0.075	0.03	0.17	0.117E-06	0.186E-11	0.116E 08	0.278E 04
400.	30.	0.080	0.10	0.32	0.612E-06	0.207E-10	0.129E 09	0.930E 04
675.	30.	0.085	0.10	0.47	0.841E-06	0.303E-10	0.189E 09	0.112E 05
727.	10.	0.080	0.10	0.45	0.728E-06	0.824E-11	0.515E 08	0.586E 04
820.	20.	0.080	0.10	0.35	0.464E-06	0.105E-10	0.657E 08	0.661E 04

OPGT PHOTO POLARIMETER PERFORMANCE FOR SATURN WITH OMEGA= 0.4000000E-05SR AND INTEGRATION TIME= 1.SEC

WAVELENGTH (NM)	DELTA WVL (NM)	DET. RESP. (A/W)	OPTICAL TRANS.	ALBEDO	SPECTRAL RAD. (W/(CM2-SR-NM))	I CATHODE (A)	COUNT RATE (C/S)	S/N RATIO
270.	50.	0.075	0.03	0.13	0.206E-07	0.454E-12	0.284E 07	0.137E 04
400.	30.	0.080	0.10	0.26	0.159E-06	0.539E-11	0.337E 08	0.474E 04
675.	30.	0.085	0.10	0.44	0.251E-06	0.907E-11	0.567E 08	0.614E 04
727.	10.	0.080	0.10	0.40	0.207E-06	0.234E-11	0.146E 08	0.312E 04
820.	20.	0.080	0.10	0.31	0.131E-06	0.297E-11	0.185E 08	0.352E 04

OPGT PHOTO POLARIMETER PERFORMANCE FOR URANUS WITH OMEGA= 0.6400000E-04SR AND INTEGRATION TIME= 1.SEC

WAVELENGTH (NM)	DELTA WVL (NM)	DET. RESP. (A/W)	OPTICAL TRANS.	ALBEDO	SPECTRAL RAD. (W/(CM2-SR-NM))	I CATHODE (A)	COUNT RATE (C/S)	S/N RATIO
270.	50.	0.075	0.03	0.41	0.200E-07	0.511E-11	0.319E 08	0.461E 04
400.	30.	0.080	0.10	0.59	0.803E-07	0.435E-10	0.272E 09	0.134E 05
675.	30.	0.085	0.10	0.35	0.445E-07	0.257E-10	0.160E 09	0.103E 05
727.	10.	0.080	0.10	0.26	0.299E-07	0.541E-11	0.338E 08	0.475E 04
820.	20.	0.080	0.10	0.12	0.113E-07	0.410E-11	0.256E 08	0.413E 04

OPGT PHOTO POLARIMETER PERFORMANCE FOR NEPTUNE WITH OMEGA= 0.6400000E-04SR AND INTEGRATION TIME= 1.SEC

WAVELENGTH (NM)	DELTA WVL (NM)	DET. RESP. (A/W)	OPTICAL TRANS.	ALBEDO	SPECTRAL RAD. (W/(CM2-SR-NM))	I CATHODE (A)	COUNT RATE (C/S)	S/N RATIO
270.	50.	0.075	0.03	0.51	0.105E-07	0.268E-11	0.167E 08	0.334E 04
400.	30.	0.080	0.10	0.61	0.350E-07	0.190E-10	0.119E 09	0.890E 04
675.	30.	0.085	0.10	0.27	0.145E-07	0.834E-11	0.523E 08	0.590E 04
727.	10.	0.080	0.10	0.19	0.924E-08	0.167E-11	0.104E 08	0.264E 04
820.	20.	0.080	0.10	0.09	0.359E-08	0.129E-11	0.812E 07	0.232E 04

OPGT PHOTO POLARIMETER PERFORMANCE FOR PLUTO WITH OMEGA= 0.6400000E-04SR AND INTEGRATION TIME= 1.SEC

WAVELENGTH (NM)	DELTA WVL (NM)	DET. RESP. (A/W)	OPTICAL TRANS.	ALBEDO	SPECTRAL RAD. (W/(CM2-SR-NM))	I CATHODE (A)	COUNT RATE (C/S)	S/N RATIO
270.	50.	0.075	0.03	0.09	0.186E-08	0.473E-12	0.296E 07	0.140E 04
400.	30.	0.080	0.10	0.10	0.575E-08	0.312E-11	0.195E 08	0.360E 04
675.	30.	0.085	0.10	0.15	0.807E-08	0.465E-11	0.290E 08	0.440E 04
727.	10.	0.080	0.10	0.15	0.730E-08	0.132E-11	0.825E 07	0.234E 04
820.	20.	0.080	0.10	0.15	0.598E-08	0.216E-11	0.135E 08	0.300E 04

OPGT PHOTO POLARIMETER PERFORMANCE FOR 100 S10 WITH OMEGA= 0.2150000E-02SR AND INTEGRATION TIME= 10.SEC

WAVELENGTH (NM)	DELTA WVL (NM)	DET. RESP. (A/W)	OPTICAL TRANS.	ALBEDO	SPECTRAL RAD. (W/(CM2-SR-NM))	I CATHODE (A)	COUNT RATE (C/S)	S/N RATIO
270.	50.	0.075	0.03	*****	0.417E-13	0.357E-15	0.223E 04	0.121E 03
400.	30.	0.080	0.10	*****	0.116E-12	0.211E-14	0.132E 05	0.296E 03
675.	30.	0.085	0.10	*****	0.108E-12	0.210E-14	0.131E 05	0.296E 03
727.	10.	0.080	0.10	*****	0.982E-13	0.597E-15	0.373E 04	0.157E 03
820.	20.	0.080	0.10	*****	0.805E-13	0.978E-15	0.611E 04	0.201E 03

TELESCOPE DIAMETER= 7.5 CM, OBSCURATION FACTOR= 0.20, AND NOISE FACTOR= 1.5

Section 4
OPTICAL DESIGN

The optical system derived for an outer planet mission photometer-polarimeter instrument during this study consists of a telescope, field defining apertures, an achromatic half-wave retarder for each passband filter, a polarization analyzer, relay-detector optics, and two detectors. See Figure 3-1.

The telescope is a Cassegrainian type with an f/4 replicated (for light weight), 3-inch diameter primary mirror. A conventional secondary mirror is suggested, however, because it is significantly smaller and the weight saving due to replication would be minimal. The computed optical parameters, a surface-to-surface ray trace, and image quality plots are shown in Table 4-1 and Figures 4-1 through 4-5. The image quality plots shown are for points at the telescope focal plane and detector-lens plane. A 3° FOV was assumed for all cases plotted. The f/4 focal ratio was chosen as the best compromise between weight (size) and desired polarimetric performance.

Pupil imaging (i.e., exit pupil of the telescope) on the detectors is implemented for the purpose of obtaining uniform photometric response across the FOV of the system. Detector surface non-uniformities which could appear as spatial scene variations are averaged over the entire FOV through this technique. This then is an important feature to eliminate a potential source of instrumental radiometric and polarimetric errors.

All mirrors are coated with aluminum overcoated with SiO_2. This is desirable because the primary mirror (which is the entrance aperture) is imaged on the detector, as described above. Therefore spatial non-uniformities or reflectance variations across the mirror surface will affect the system performance in the same way as the photocathode variations discussed above. The cathode is effectively projected on these mirror surfaces by the pupil imaging scheme. Figure 4-6 shows the dependence of linear polarizance produced by reflection from such a mirror with an aluminum coating. The

Table 4-1. Photometer-Polarimeter Computer Design: Optical Parameters and Ray Trace

OPTICAL PARAMETERS

PHOTO-POLARIMETER [illegible] DEC 71 OPGT f/4

SURF	ITAG	RADIUS	T	N(D)	N(F)	N(C)
1	1	-15.00000	-3.75000	-1.00000	1.00000	1.00000
0.000000E 00		0.0000000 00	0.0000000 00		0.0000000E 00	-0.5500000E 00
2	1	-45.00000	4.48500	1.00000	1.00000	1.00000
3	1	**********	0.03000	1.00000	1.00000	1.00000
4	1	**********	0.15000	1.39000	1.41000	1.38000
5	1	**********	0.50000	1.00000	1.00000	1.00000
6	1	2.00000	1.12500	1.46000	1.51000	1.45000
7	1	**********	1.10000	1.00000	1.00000	1.00000
8	1	3.00000	0.12500	1.46000	1.51000	1.45000
9	1	-2.25000	0.70000	1.00000	1.00000	1.00000
10	1	**********	0.50000	1.00000	1.00000	1.00000
11	1	**********	0.58000	1.00000	1.00000	1.00000

SYSTEM DATA (K=31 TO 34, EFL, ENT)

0.000000 1.500000 0.028000 0.000000 1.000000 1.000000 1.000000

11 1 1 1 0.0000 0.0000 0.5800 1.0000 0.0000

RAY DATA (K=31 TO 45)

1 S 0.00000 1.50000 0.30000 0.00000

1.00000 0.30000 0.00000

SURFACE-TO-SURFACE RAY TRACE

SURF	X	Y	Z	TAN X	TAN Y	TAN XY	
1	THETA = -1.500000 DEG						
1	0.000000	1.501971	-0.0752	0.0000	0.2301	0.2301	Top of Entrance Pupil
2	0.000000	0.855077	-0.0047	0.0000	-0.1997	0.1997	
3	0.000000	-0.242544	0.0000	← Focal Plane			
4	0.000000	-0.249535	0.0000				
5	0.000000	-0.289881	0.0000				
6	0.000000	-0.376889	0.0358	0.0000	-0.0718	0.0718	
7	0.000000	-0.455103	0.0000	0.0000	-0.1051	0.1051	
8	0.000000	-0.576252	0.0555	0.0000	-0.0091	0.0091	
9	0.000000	-0.578590	-0.0751	0.0000	0.1108	0.1108	
10	0.000000	-0.498702	0.0000				
11	0.000000	-0.439295	0.0000	0.0000	0.1108	0.1108	
IM	0.000000	-0.371024	0.5800	0.0000	0.1108	0.1108	
1	0.000000	0.000000	0.0000	0.0000	0.0261	0.0261	Center of Entrance Pupil
2	0.000000	-0.098200	-0.0001	0.0000	-0.0305	0.0305	
3	0.000000	-0.235390	0.0000				
4	0.000000	-0.236306	0.0000				
5	0.000000	-0.239603	0.0000				
6	0.000000	-0.255880	0.0168	0.0000	0.0196	0.0196	
7	0.000000	-0.233578	0.0000	0.0000	0.0287	0.0287	
8	0.000000	-0.201793	0.0067	0.0000	0.0408	0.0408	
9	0.000000	-0.197313	-0.0086	0.0000	0.1010	0.1010	
10	0.000000	-0.125731	0.0000				
11	0.000000	-0.075226	0.0000	0.0000	0.1010	0.1010	
IM	0.000000	-0.016681	0.5800	0.0000	0.1010	0.1010	
1	0.000000	-1.498038	-0.0746	0.0000	-0.1751	0.1751	Bottom of Entrance Pupil
2	0.000000	-0.853106	-0.0080	0.0000	0.1362	0.1362	
3	0.000000	-0.240198	0.0000				
4	0.000000	-0.238111	0.0000				
5	0.000000	-0.221472	0.0000				
6	0.000000	-0.152540	0.0058	0.0000	0.1173	0.1173	
7	0.000000	-0.021231	0.0000	0.0000	0.1726	0.1726	
8	0.000000	0.169519	0.0047	0.0000	0.0988	0.0988	
9	0.000000	0.180688	-0.0072	0.0000	0.1073	0.1073	
10	0.000000	0.258609	0.0000				
11	0.000000	0.310282	0.0000	0.0000	0.1073	0.1073	
IM	0.000000	0.372542	0.5800	0.0000	0.1073	0.1073	

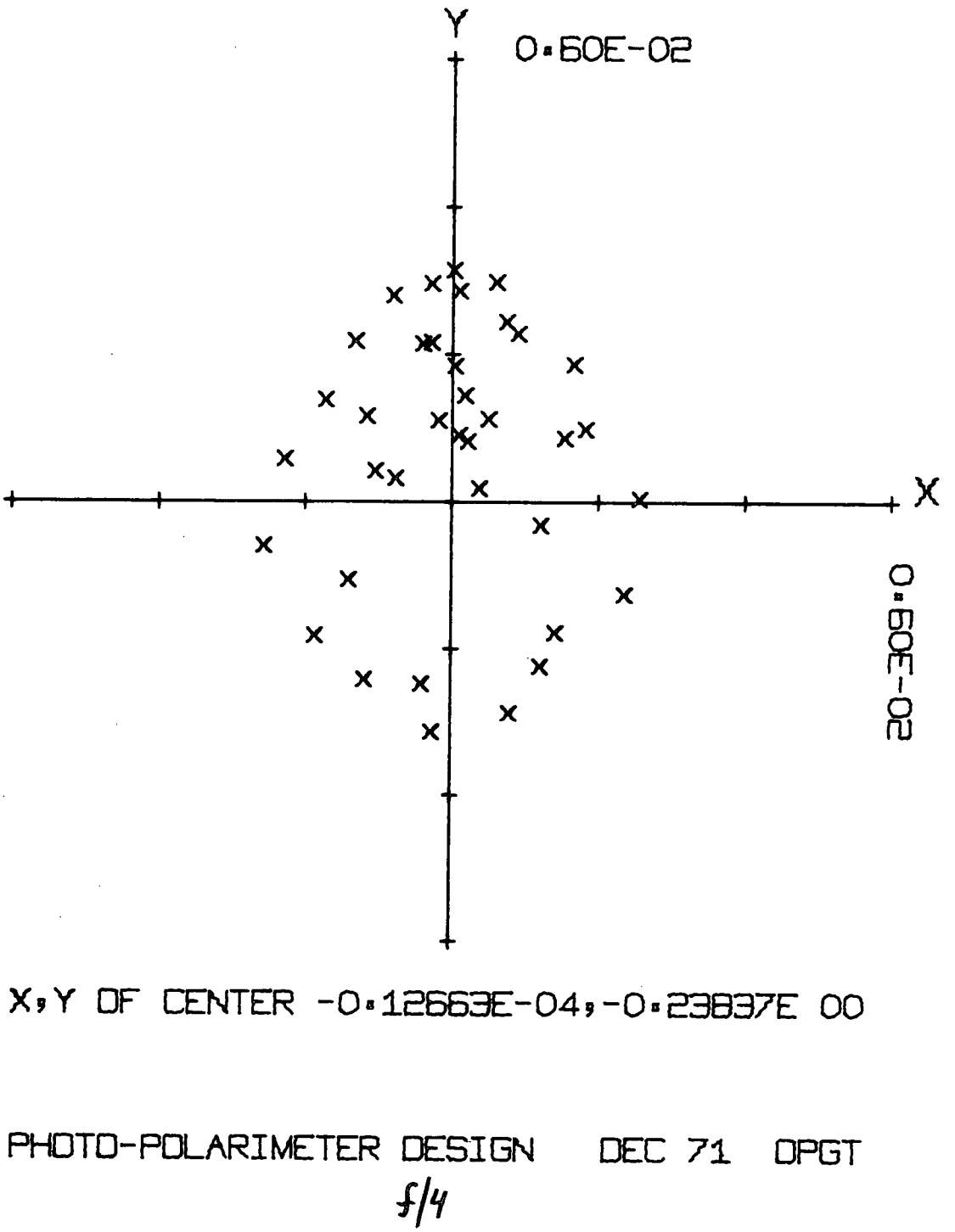

Figure 4-1. Photometer-Polarimeter Optical Design: Telescope Image Plane Spot Diagram

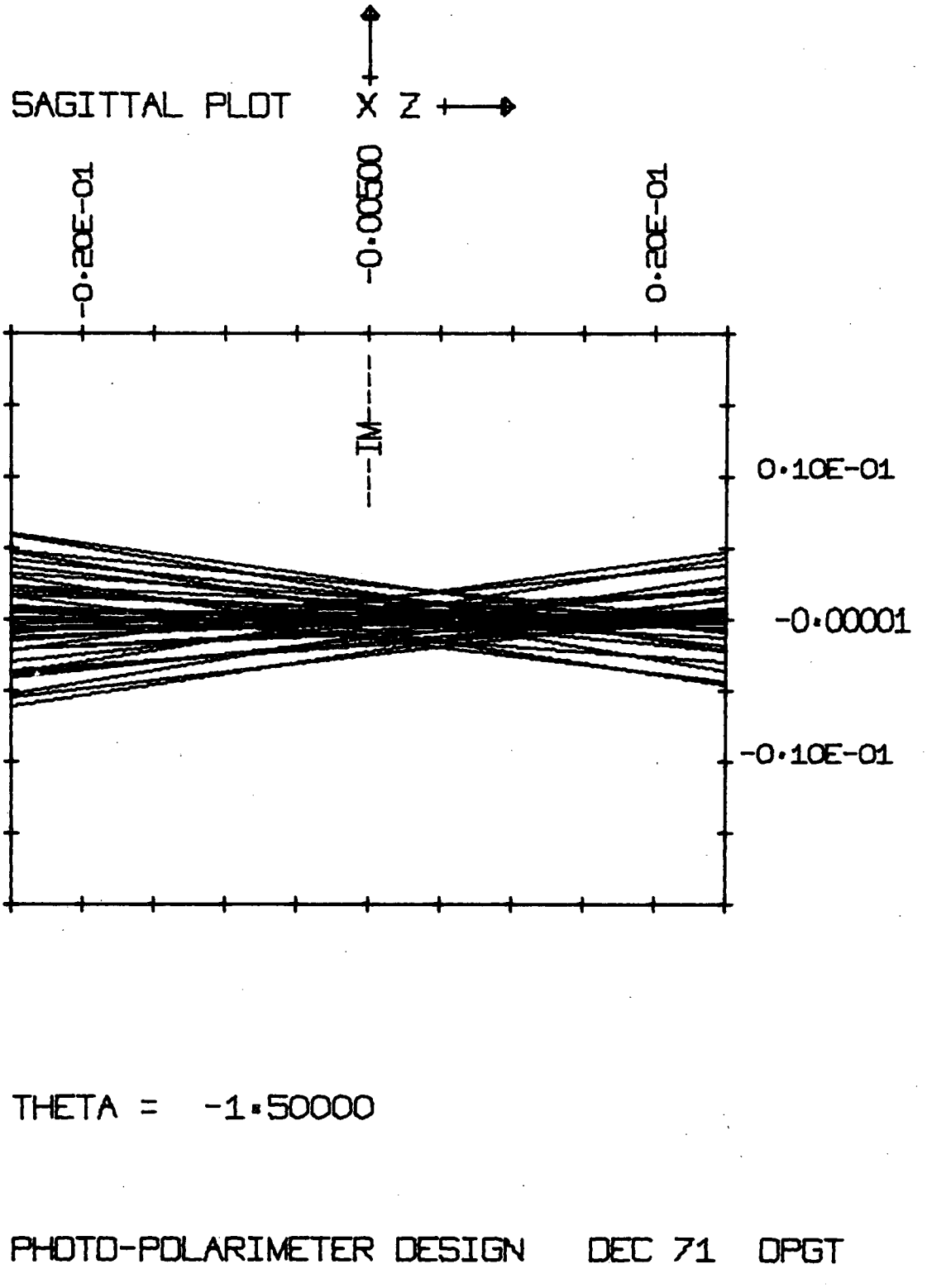

Figure 4-2. Photometer-Polarimeter Optical Design: Telescope Image Plane Sagittal Ray Trace Plot

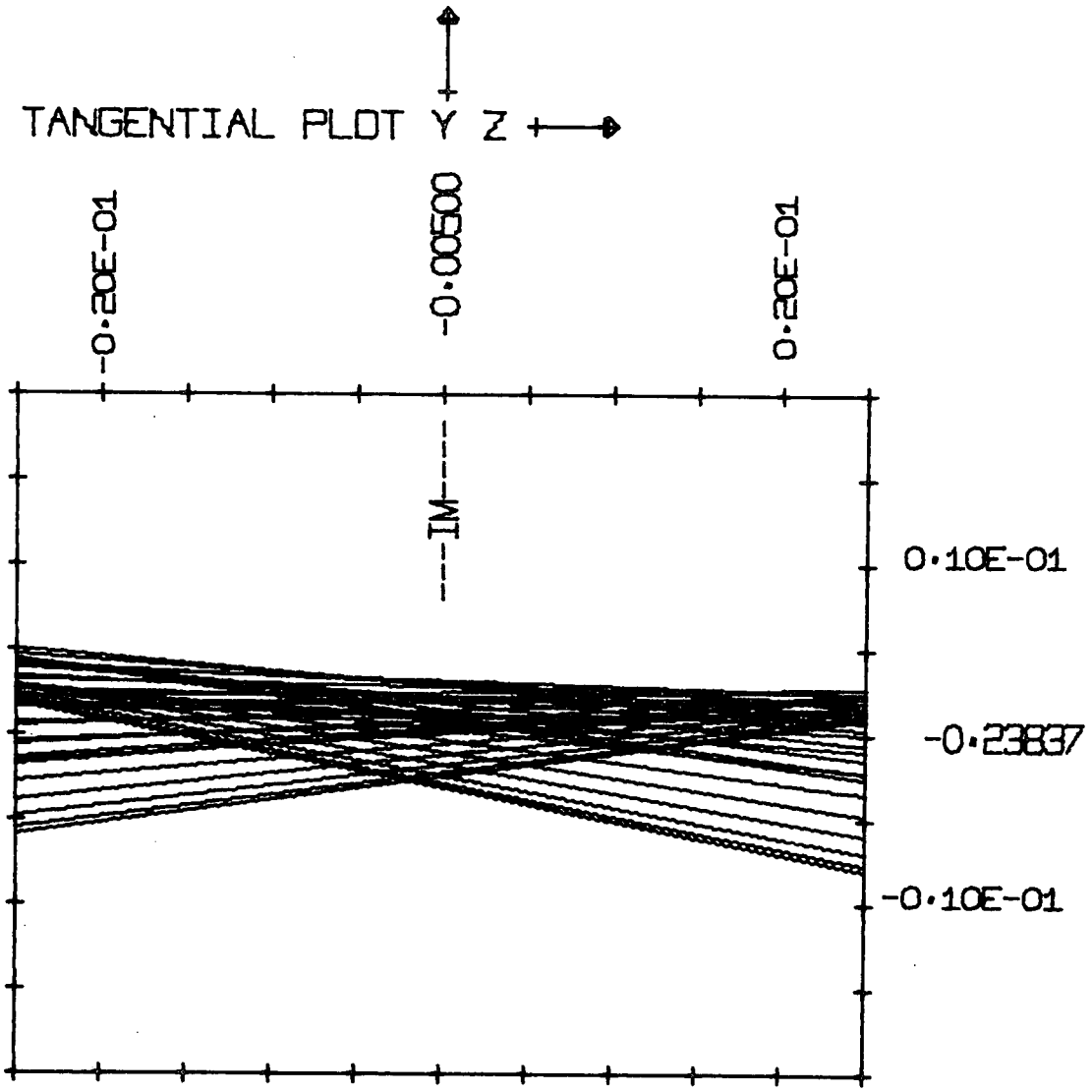

Figure 4-3. Photometer-Polarimeter Optical Design: Telescope Image Plane Tangential Ray Trace Plot

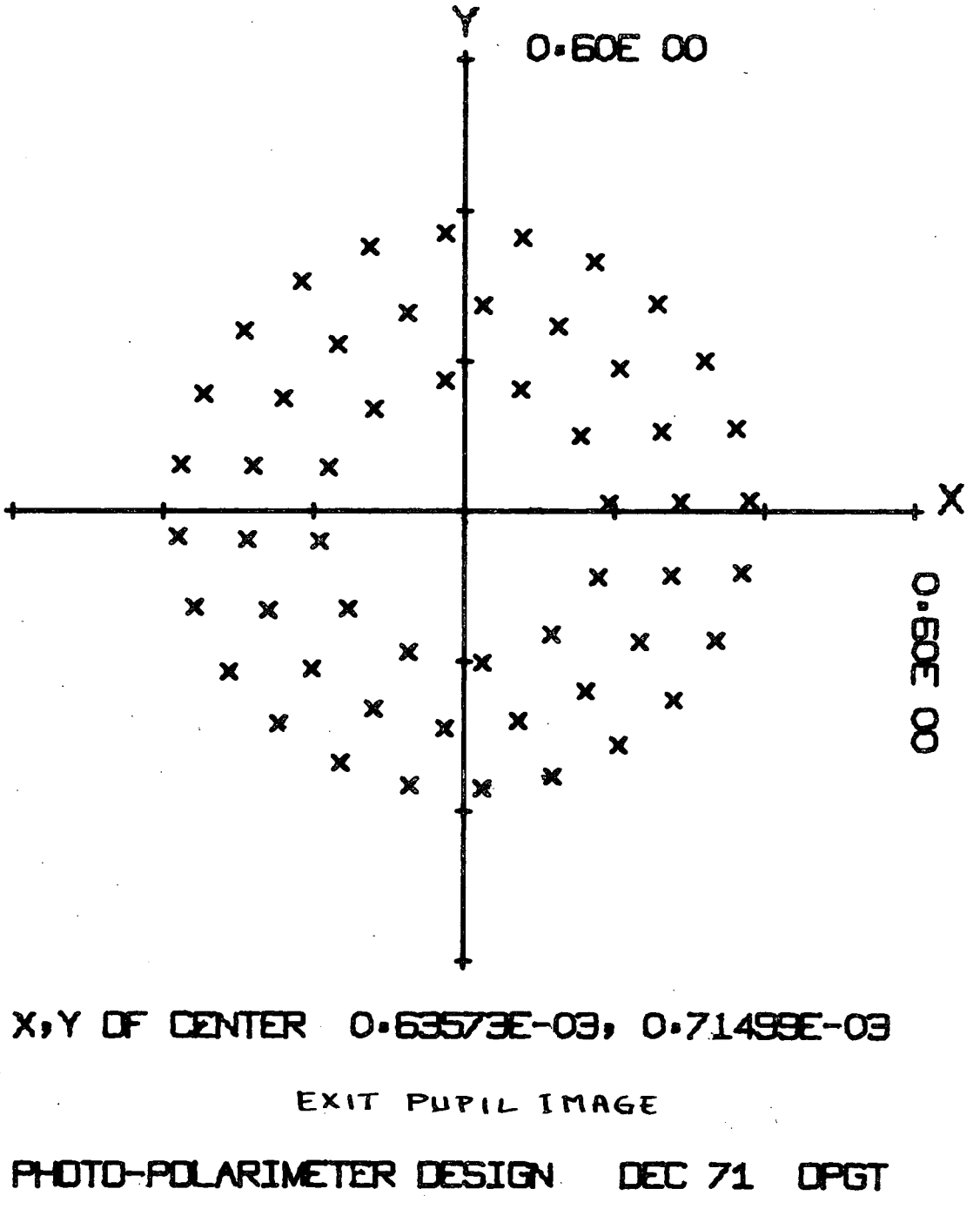

Figure 4-4. Photometer-Polarimeter Optical Design: Detector-Lens Image Plane Spot Diagram

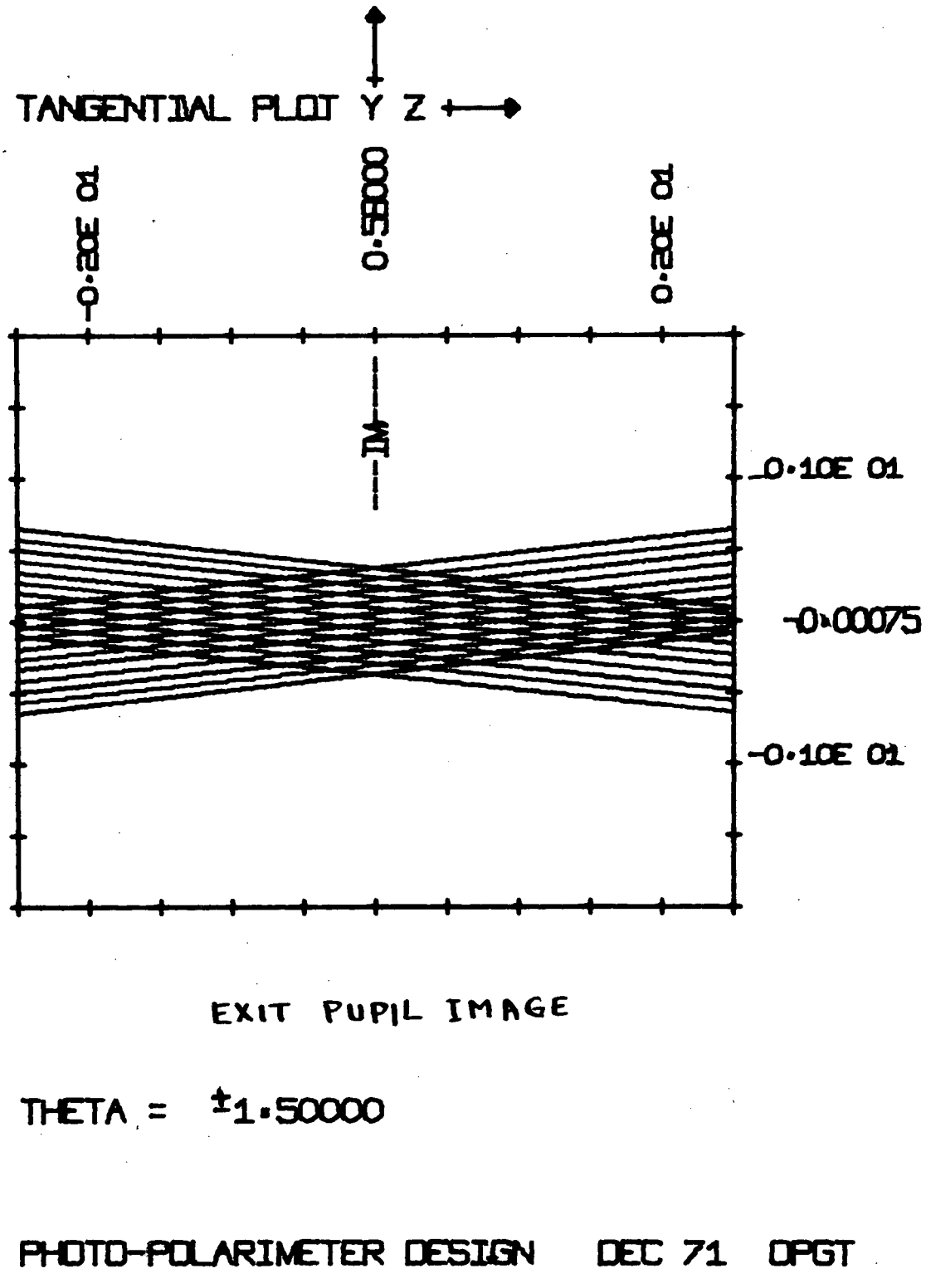

Figure 4-5. Photometer-Polarimeter Optical Design: Detector-Lens Image Plane Tangential Ray Trace Plot for Two Extreme Field Angles

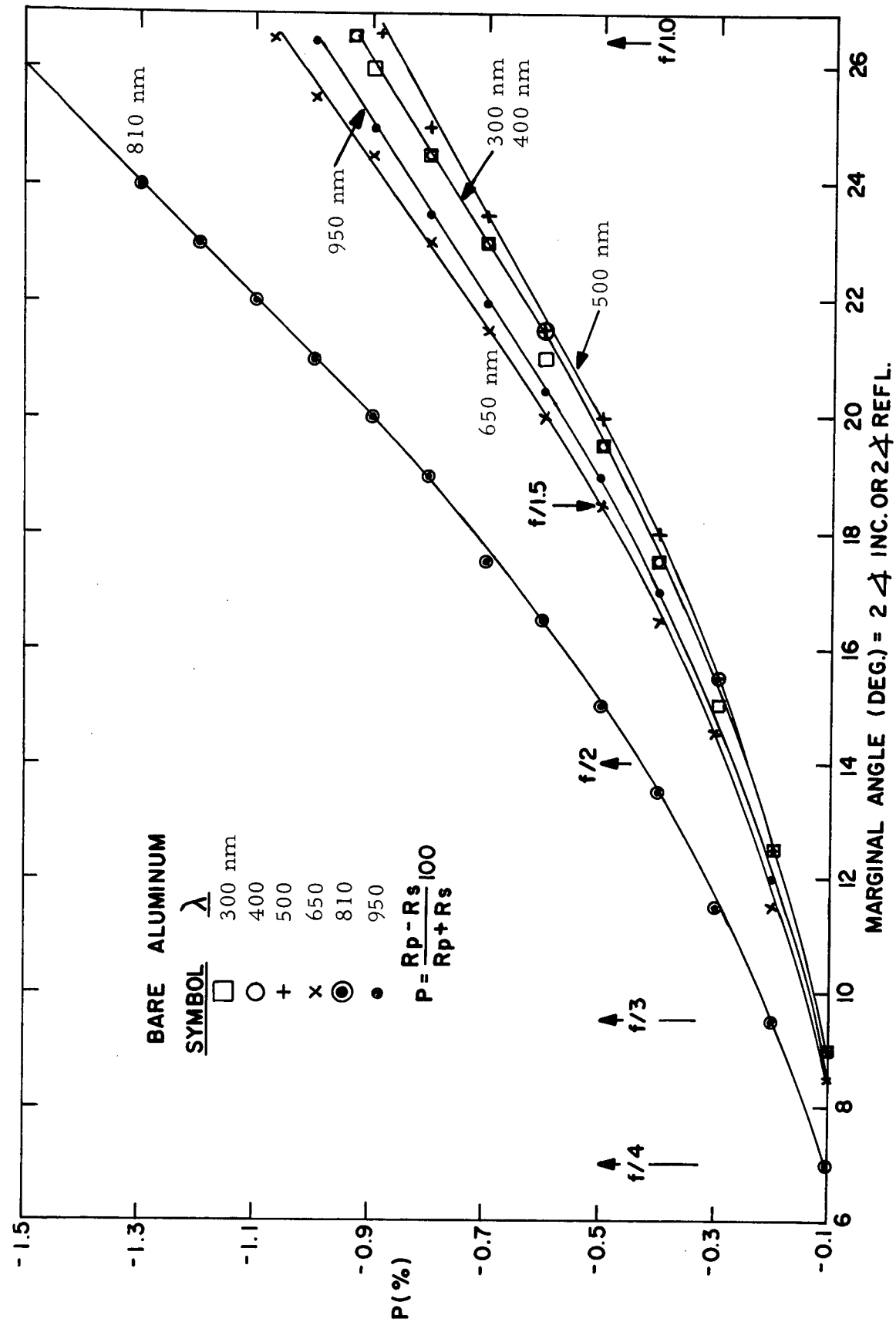

Figure 4-6. Computed Dependence of Linear Polarizance on Angle of Incidence for an Aluminum Coating

curves are for reflection at different angles and for several wavelengths. These plots were calculated using a computer program for thin-film design developed by SBRC. It is evident that intrinsic polarizance (systematic instrument error) can indeed exist when non-isosensitive detector cathodes are used in a system with fast mirrors. The magnitude of this error is of course dependent on the lack of cathode isosensitivity, either real or induced by the preceding mirrors. This value is small, usually on the order of $< 0.4\%$ polarizance.

An aperture actuator (similar to one previously used in the Pioneer F/G Imaging Photopolarimeter) is located at the telescope focal plane. This actuator inserts field stops of various sizes and appropriate calibration sources into the optical system. Two calibration sources are used; a diffuse surface to scatter light from an incandescent lamp, and a radioisotope-actived-phosphor to simulate faint objects. (Similar internal calibration was used for the Pioneer F/G IPP Instrument.)

A third possibility for absolute calibration is to provide for a view of the sun through a suitable photometric attenuator. An attenuation of approximately 10^7 is required to reduce the direct sunlight to an acceptable radiance level with the exact value dependent on the albedo to be simulated. Calculations with the SBRC Thin-Film Computer Program indicate that such an attenuator is technically feasible. However, further investigation of the effect of residual heat generation through attendant absorption is necessary before the practical feasibility can be definitely established.

A second actuator (Filter-Retarder Assembly) carries bandpass filters, each in combination with an achromatic half-wave retarder. This technique allows significant simplification over the broadband achromatic half-wave retarder used over the 400-700 nm spectral range covered by the IPP instrument. In the previous broadband case, one is constrained to the use of a delicate and complex AHWR of the Pancharantnam design in which a half-wave retarder is mounted at a specific angle between two outer half-wave retarders oriented with their axes parallel. Although a single material is used (MgF_2),

for this "sandwich," the direction of the optic axis of the combination is dependent on wavelength.[1] Figure 4-7 shows the angular deviation versus wavelength for the IPP flight spare AHWR with the incident polarization vector at an arbitrary angle of 25°.

The much simpler AHWRs recommended for the Jupiter-Saturn mission would consist of half-wave elements constructed of MgF_2 and sapphire, each optimized for a relatively narrow spectral band.[2] This simplified concept requires that the actuator step in 22.5° increments with each single filter/retarder covering three 22.5° positions (Figure 3-1). Thus incoming light may be sequentially retarded 0°, 45°, and 90° in each of the spectral bands with an approach that greatly simplifies the assembly and alignment of the retarders. Furthermore, at the 90° retardance position the roles of the detectors and analyzing optics are interchanged. This redundancy allows any existing instrumental sensitivity to orthogonal planes of polarization to be calibrated. Selection of specific materials used in the fabrication of the filter substrates and retarders will be discussed in a following Radiation Tests Section.

Following the focal plane optics a positive lens of fused silica is used to reduce the divergence angle of the f/4 beam. The reduced divergence angle through the analyzer section simplifies the design of this critical portion of the optical system.

Two choices of an analyzer-beam splitter were considered; a Wollaston prism similar to one used for the IPP, and a multilayer thin-film (MacNeille) beam splitter. A birefringent Wollaston prism has the advantage of yielding the most complete polarimetric analysis of the light beams that is now possible. However, to obtain adequate physical deviation of the resultant beams (α) it is necessary to use a material which exhibits a large birefringence since $\alpha \propto |n_e - n_o|$. Table 4-2 lists the birefringences of ten crystals usable over a wide range of spectral wavelengths. It is evident that over the wavelength

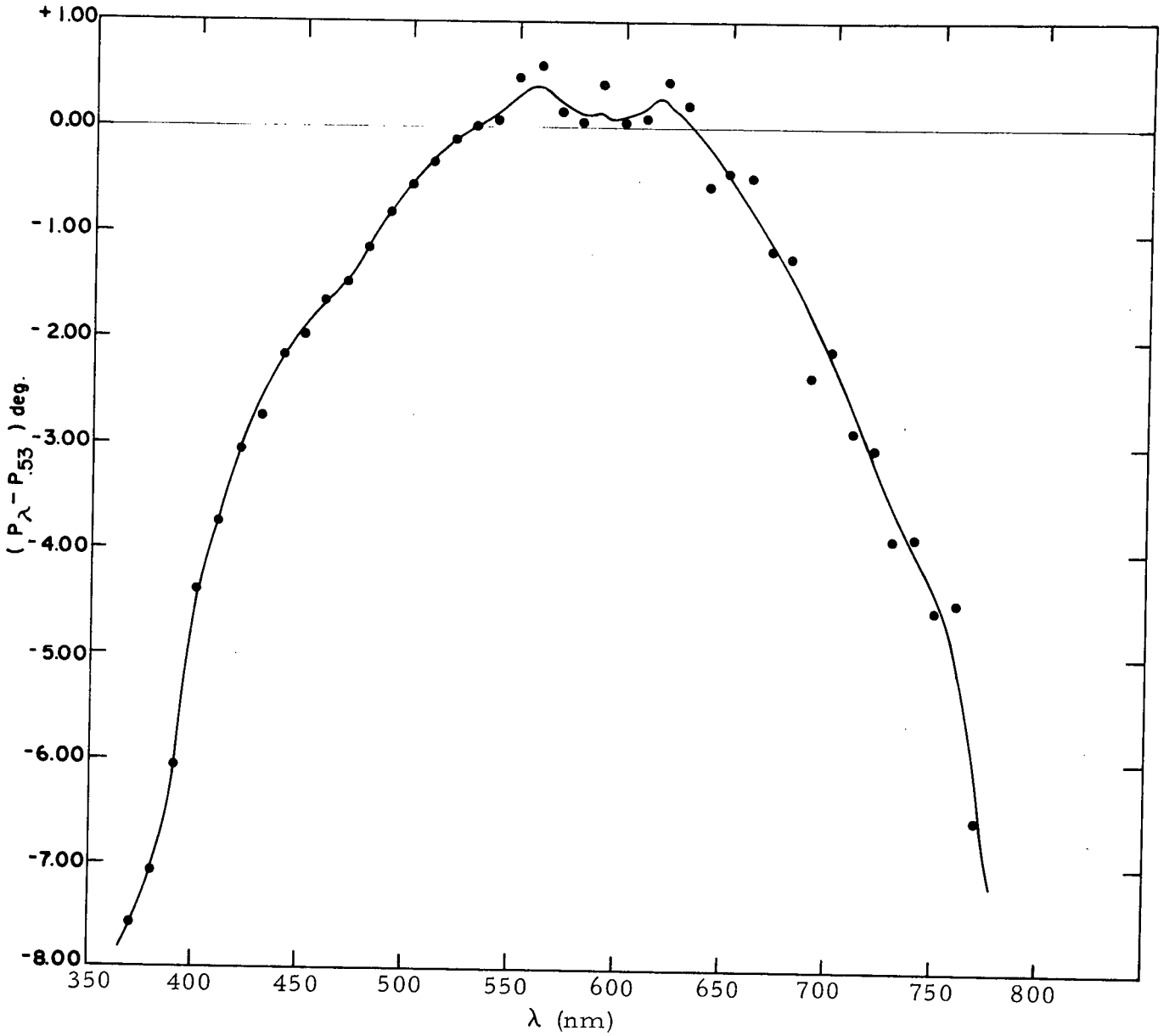

Figure 4-7. Wavelength Dependence of the Deviation in Retardance for the MgF_2 Achromatic Half-Wave Retarder Used in the Pioneer Imaging Photopolarimeter (Flight Spare)
Incident Polarization Angle = 25°

Table 4-2. Birefringent Crystals for Polarization Optics

Wavelength Region (nm)	Crystal	Vis. Birefring. ($n_e - n_o$)	Radiation Stability	Comments
130-7000	MgF_2	+0.011	Excellent	Easy to work
170-3500	Quartz	+0.009	Must Select	No advantage over MgF_2
240-5000	$CaCO_3$	-0.172	Must Select	Sensitive to thermal shock
400-5000	YVO_4	+0.226	Good	Not available in sizes >1 cm^2, Easy to work
440-5000	TiO_2 (Rutile)	+0.305	?	
200-1300	ADP	-0.05	Good (?)	Soluble, sensitive to thermal shock
450-5000	$LiNbO_3$	-0.10	?	
150-6000	Al_2O_3 (Sapphire)	-0.008	Good	
190-9000	LaF_3	-0.008	?	Size available ?
200-310 and 450-520	$NiSO_4$	-0.02	?	Soluble, Optically Active

region from 250 to 800 nm only calcite exhibits sufficient birefringence to obtain adequate deviation through a small prism.

Experience gained with previous instruments, and especially during development of the IPP, has revealed that calcite prisms require special attention and handling because of an inherent sensitivity to thermal shock and sustained extreme temperatures. This sensitivity results from the large anisotropic thermal expansion coefficient characteristics of birefringent materials. When the axes of the crystal segments which constitute the prism are arranged orthogonally, thermally induced forces occur at the interfaces in shear and tension.

Another problem inherent with natural calcite is the presence of impurities which cause defects in the lattice sites and render the crystal susceptible to discoloration when bombarded with high energy radiation. Because it is a naturally occurring material it is necessary to select calcite through a testing process. Selection was done by subjecting a small piece of a larger crystal to particle and gamma irradiation, then measuring the resultant spectral change in optical transmission. Calcite materials have been so tested which have exhibited no (< 5%) change in transmission after 10^6 rad of 10 Mev electron irradiation. In contrast, other samples of calcite became orange colored and phosphoresced brightly for at least 20 hours. Such behavior, due to trace impurities in the calcite, is impossible to predict apriori.

Fluorescence during irradiation is also a likelihood with all transparent materials. No tests were made to detect fluorescence however. The recent announcement that the "Laboratories Electronique et de Physique Appliquees" in Limeli-Brevannes, France, has produced artificial calcite 2 to 3 cm long may hold some promise in obtaining purer crystals for future needs.[3]

A difficulty inherent in all birefringent beam splitters is the dependency of birefringence on spectral wavelength. Such spectral dispersion was investigated for several construction angles using a compensated Wollaston prism (Figure 4-8). Dispersion values were calculated from the approximate formula

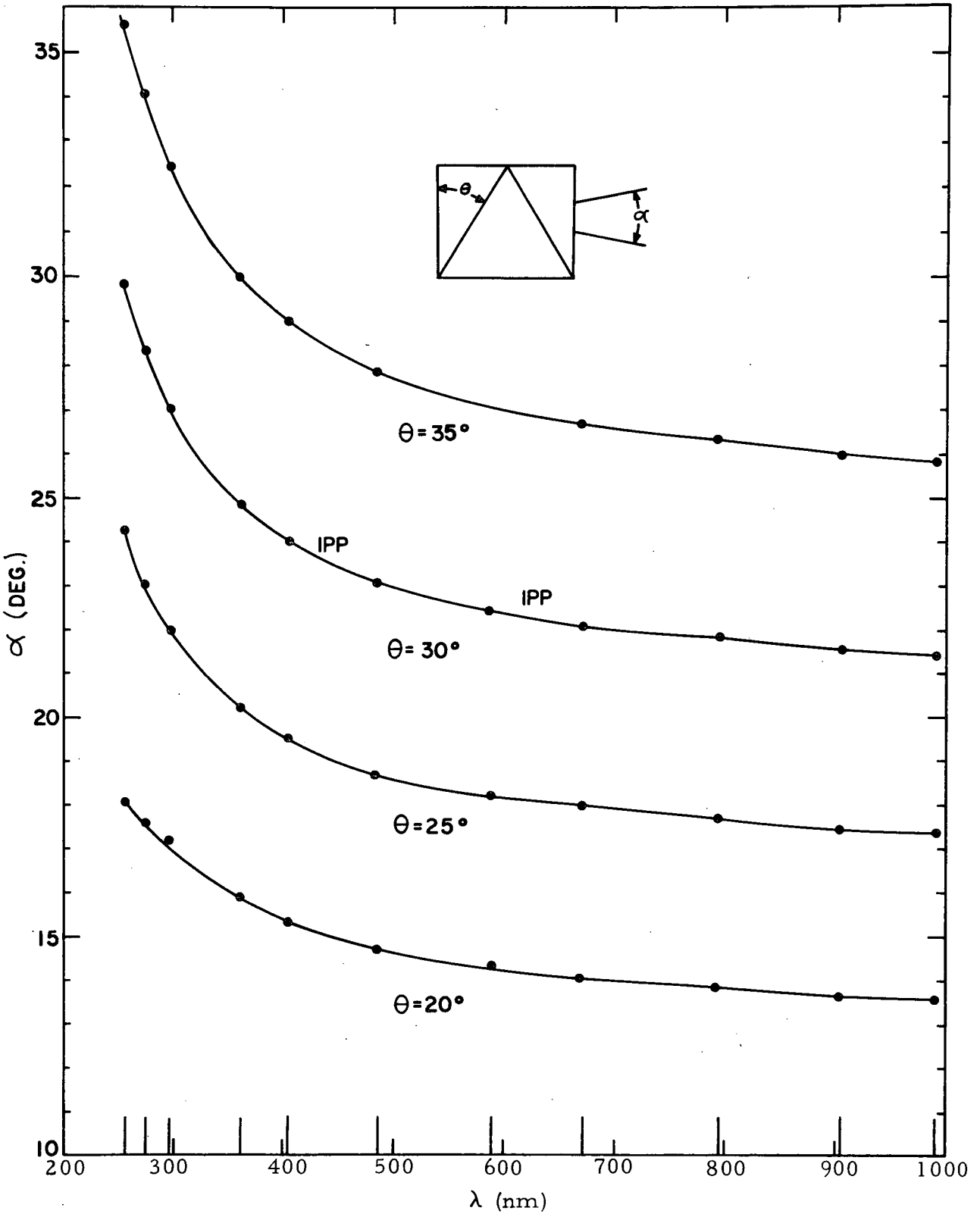

Figure 4-8. Dispersion of the Deviation Angle Between Orthogonally Polarized Beams for Calcite Wollaston Prism of Four Construction Angles

$\alpha \cong 2 \tan^{-1}[(N-1)|n_o - n_e| \tan \theta]$, where N = number of segments.[4] Therefore, it was shown that to use a birefringent prism over a large wavelength span, a detector with large photocathodes must be used. For example, a 30° prism operating from 250 to 900 nm placed 3 inches distant from a photocathode subtends at least 0.42 inch in the dispersed direction (plus the size of the image). The deviation due to dispersion of the reflected beam for a thin-film analyzer, by comparison, will be only 1° over the broadband range of 250 to 900 nm.

A thin-film polarizing beam splitter does not suffer from the previously described temperature, radiation, or dispersion problems. However, the thin-film analyzer is somewhat deficient in that polarimetric analysis of the orthogonal components is not complete. This is particularly true for the reflected beam which becomes less completely analyzed with increasing incidence angle.

The thin-film beam splitter interface is coated with multilayer high-reflectance stacks which are designed to be at Brewster's angle over the passbands of interest. However, analysis of the orthogonal components is not complete, particularly for the reflected beam. This defect is dependent upon the angle of flux incidence, which implies that a "slow" optical system must be used with this type device.[5, 6] The stacks reflect the s component nearly perfectly, but allow the p component to be transmitted freely.

The thin-film stacks also are efficient at higher orders of reflectance. Thus, if the analyzer is good near λ_1 it is also good at $\lambda_1/2$. An analyzer using this principle, a thin-film polarizing beam splitter designed to work in the bands (bandwidth): 270 nm (50 nm), 400 nm (30 nm), 540 nm (30 nm), 727 nm (10 nm), and 820 nm (20 to 30 nm) was procured and evaluated. Preliminary measurements of this prism are shown in Figures 4-9, 4-10, and 4-11.

Figure 4-9 shows the angular dependence of the polarizance for the transmitted beam of the prism as measured with a He-Ne laser. Internal reflections within the prism caused reduced polarizance values in the left-hand portion of the figure. Similar data are shown in Figure 4-10 for a

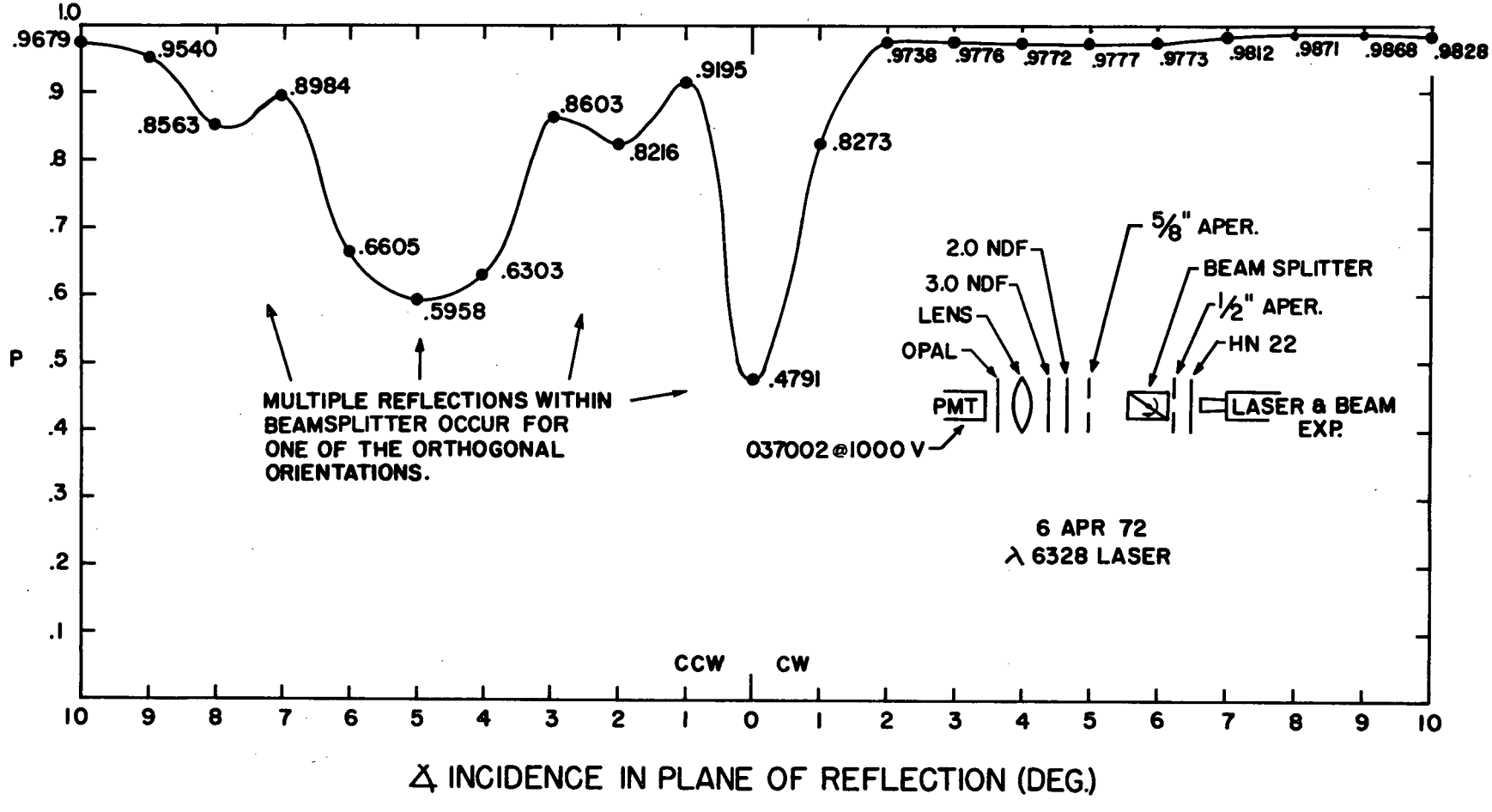

Figure 4-9. Dependence of Polarizance on Angle of Incidence for a Thin-Film Polarizing Beamsplitter (He-Ne Laser). Transmitted Beam Data Shown. (At Counterclockwise Angles Internal Reflections Appearing in One of the Orientations Reduces the Polarizance.)

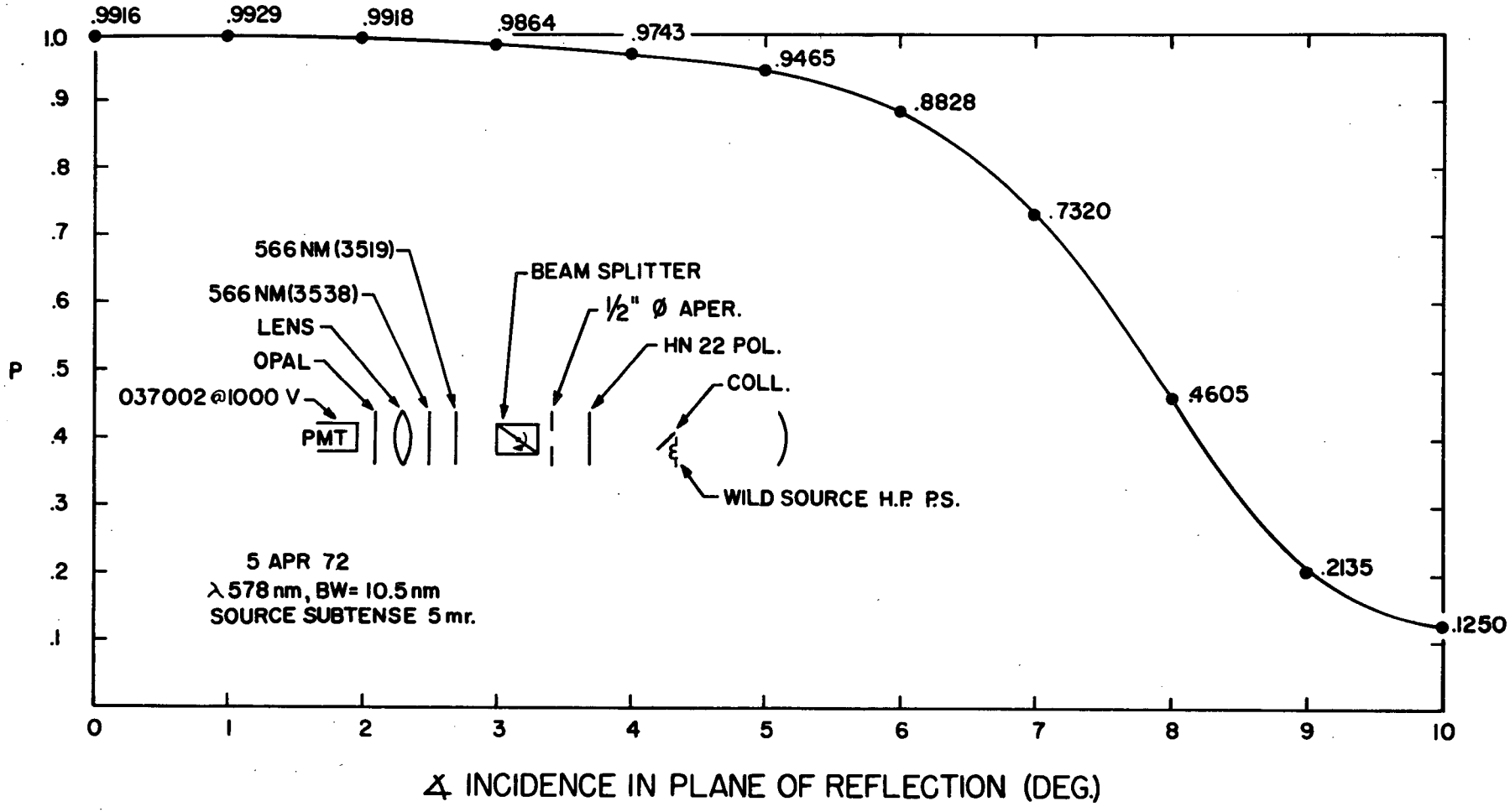

Figure 4-10. Narrow Band Polarizance vs Angle of Incidence for Thin-Film Polarizing Beamsplitter. Transmitted Beam Data Shown. One-Half of Curve Shown: Performance is Symmetrical for Clockwise and Counterclockwise Incidence.

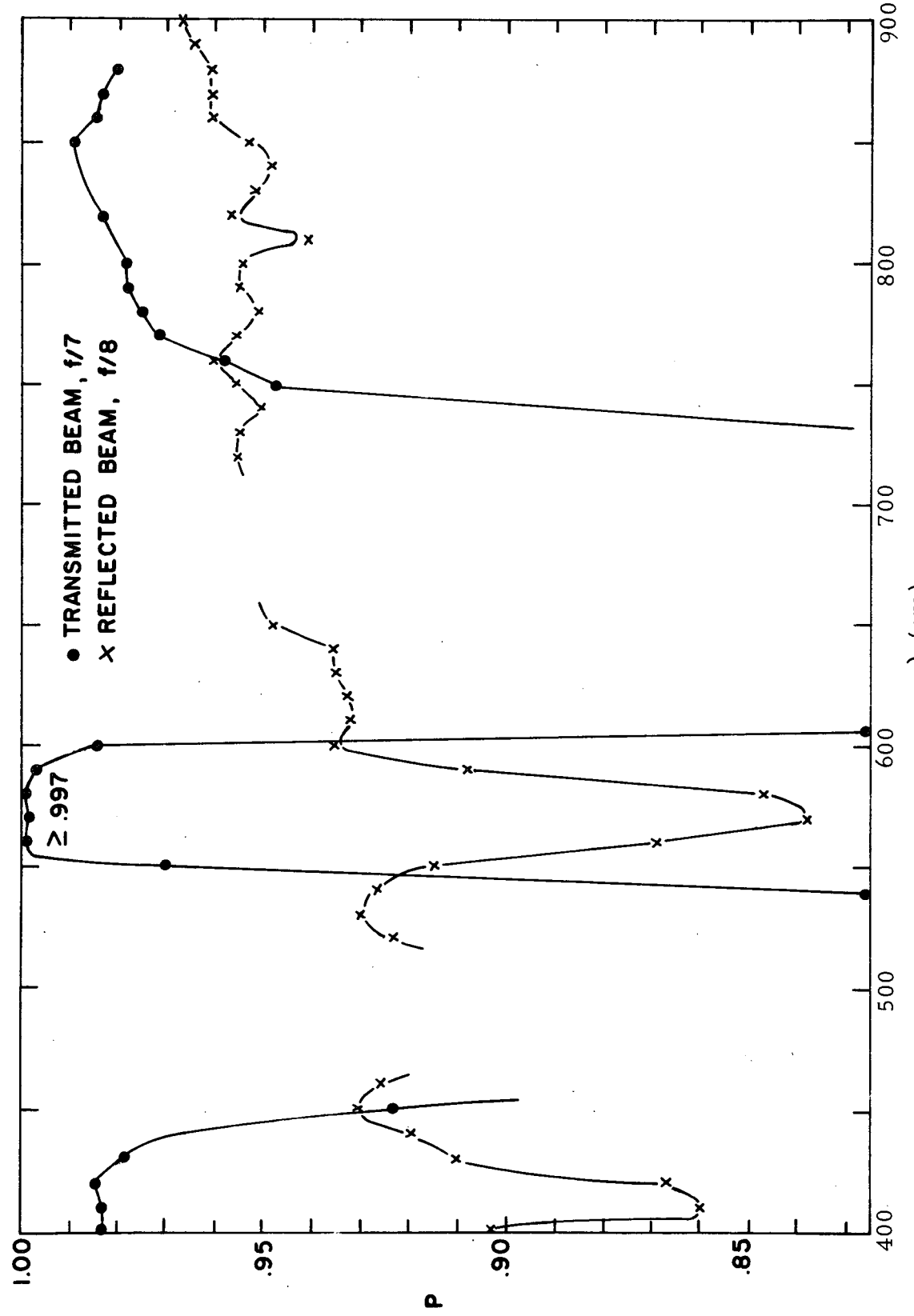

Figure 4-11. Spectral Polarizances of the Transmitted and Reflected Beams for Thin-Film Polarizing Beamsplitter

narrow spectral band centered at 578 nm with a 10.5-nm half-width. Figure 4-11 shows the spectral polarizances of both the reflected and transmitted beams with the incident flux distributed over f/8 and f/7 cones, respectively. Following these measurements, the prism was returned to the vendor with a request to re-cement the assembly with a UV transmitting bonding agent. SBRC has identified through previous testing and evaluation a UV transmitting, radiation resistant, flexible bonding agent suitable for either calcite or glass. This agent was used for the IPP calcite prisms and the thin film polarizer. Performance of the re-cemented prism is displayed in Figure 4-12.

The polarizance of the reflected beam will be between 0.90 and 0.96. This value may be increased to >0.995 with the use of a supplementary polarizer such as a Polacoat 105 UV. However, an additional transmission loss would be incurred and the overall optical transmittance would be reduced to between 40% and 30% (UV) of the transmission of the unaided beam splitter (which is 80 to 90% for each polarizance). For maximum optical efficiency, therefore, an unaided beam splitter could be used by calibrating the incomplete polarization as a systematic error. However, if sufficient light is available, greater accuracy may be attained through the use of an additional polarizer, remembering that the reflected beam will contain less energy than the transmitted beam.

It would be more efficient to use a second thin film coating on a disk which is mounted at the proper angle with respect to the reflected beam. Because the beam entering the analyzer is nearly collimated by the lens, the remaining incidence angle is due only to the field angle. Obviously, the polarizance is increased as smaller field angles are approached.

The polarizance of the transmitted beam averages 98.3% near 400 nm and 850 nm. This is lower than desired. Two errors can be responsible for the deficiency. Wide-band coverage — 710 to 850 nm — requires many layers in the contiguous high reflectance stacks. Slight errors in the centering of these stacks which cause the reflectance bands to either overlap or to be noncontinuous can cause "leaks" in the reflectance band. Errors in the phase

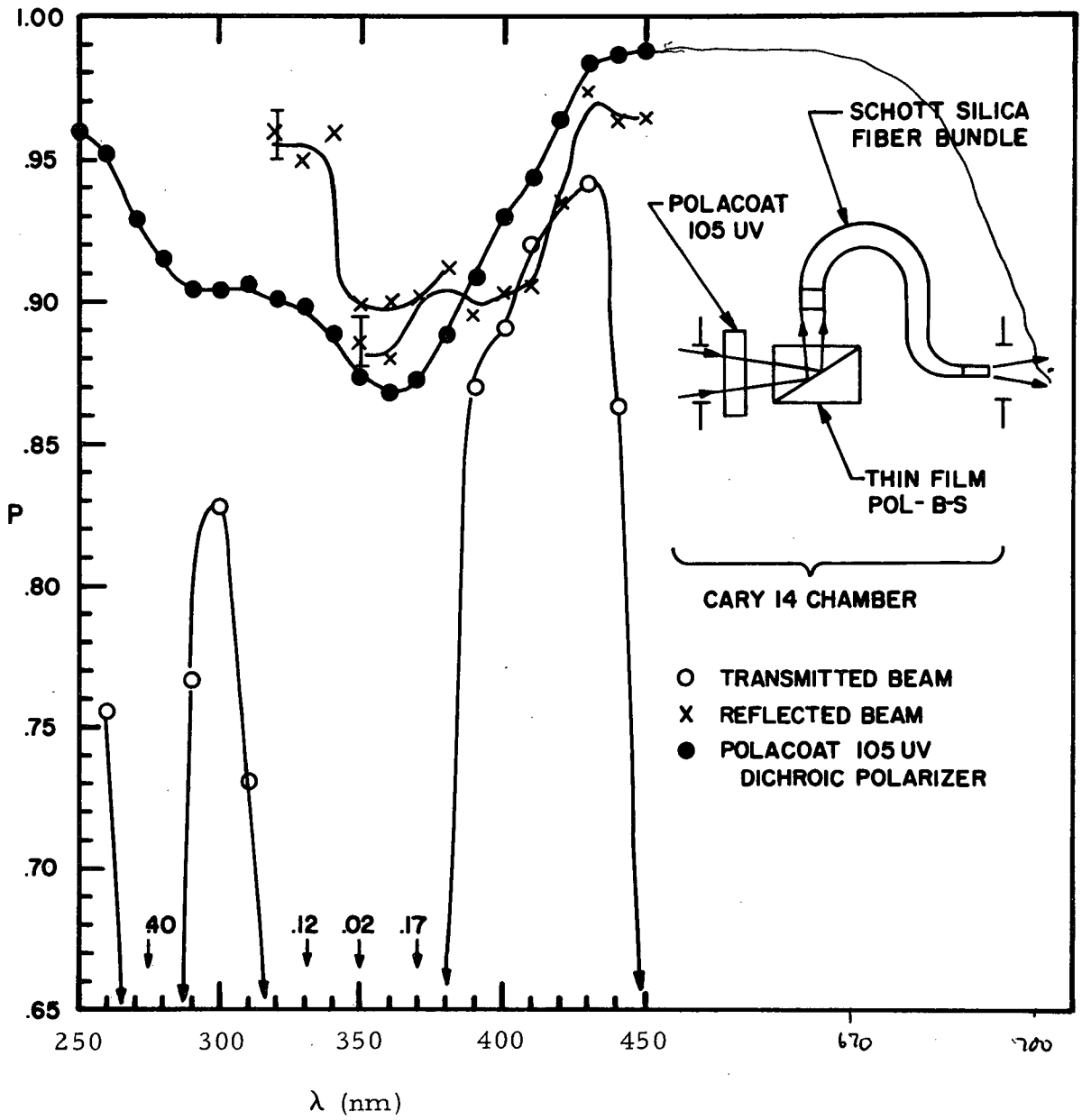

Figure 4-12. Spectral Polarizance of Thin-Film Polarizing Beam-Splitter After Re-cementing with UV Bonding Agent

The multilayer evidently is highly absorbing below 290 nm. (The cement is 50% transmitting below 260 nm.) Low signal for the reflected beam below 350 nm with the arrangement shown make those measurements uncertain. The results for the transmitted beam were corrected for the Polacoat deficiency. Cary 14 beam is f/7.

thickness of each multilayer stack also reduce the reflectance efficiency. Apparently these are the problems that have been encountered in the construction of our beam splitter. It should be possible to achieve a polarizance as high as 99.98% over 50-nm bands on future attempts. The cost of this first attempt at producing such a polarizer was $950. This is twice the cost of a flight quality IPP calcite prism.

DETECTOR POLARIZATION SENSITIVITY

Because each detector will be sensing completely polarized light, it is important to determine the effect of such polarized light flux on the spectral response and signal level of a selected photomultiplier (PMT). A side-looking GaAs PMT (RCA) was illuminated with monochromatic light from a Cary 14 Monochromator. A polarizer appropriate for the spectral region in question was rotated 90° to measure the response at each wavelength. The signal level at each wavelength was ratio'd to a spectrally calibrated silicon photodiode which possessed negligible polarization sensitivity. This diode was used to establish the polarized radiance of the monochromator, folding mirror, and condensing lens at each wavelength. The resultant plot of tube anode current as a function of polarization angle is shown as solid curves in Figure 4-13. The wavelength shift is not significant if the longest wavelength used is at least 20 nm short of the band gap edge. It may be noted that for maximum efficiency, it is important to orient the cathode properly with respect to the polarization direction.

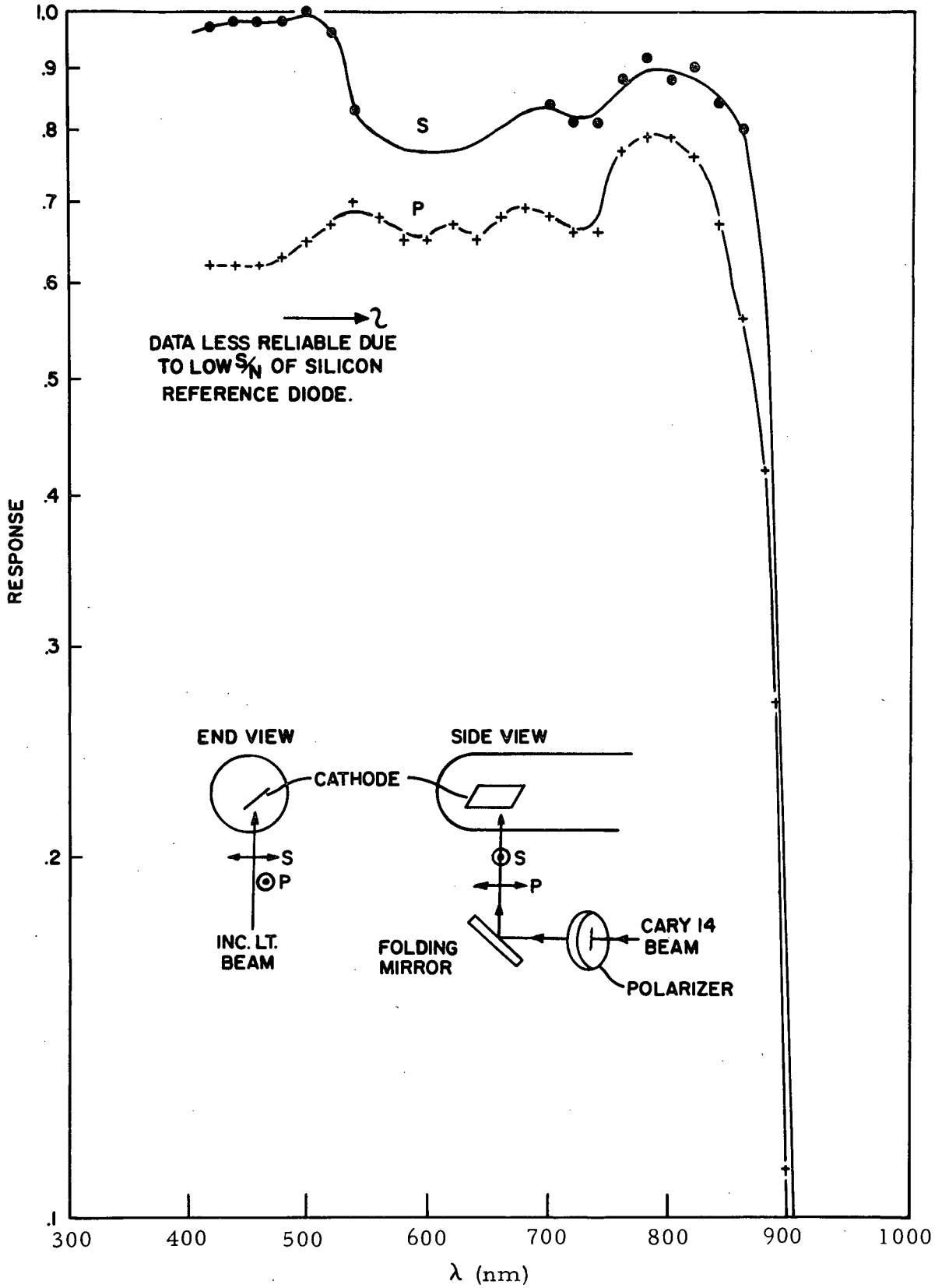

Figure 4-13. Spectral Response to Orthogonal Planes of Polarization of the RCA C31025J Photomultiplier (GaAs)

The polarization sensitivity was redetermined seven months later at a date which was one week after the tube had accumulated a 10^6 rad (Si) dosage in a cobalt 60 chamber. Table 4-3 contains these results obtained with narrow-band filters. It is believed that the small differences in magnitude of the polarization sensitivity between this data and the data of Figure 4-12 are due to differences in the angle of incidence on the cathode for the two experiments. The data in Table 4-3 are for the angle of incidence giving maximum signal. This is closer to the situation sought in actual practice. The larger differences at $\lambda < 460$ nm are due to poor signal/noise for the silicon reference diode. A preliminary determination of the spectral responsivity (not shown) indicated that no significant changes were due to irradiation.

Table 4-3. Polarization of RCA C31025J (GaAs) After 10^6 Rad Gamma Radiation**

λ (nm)	BW (nm)	P
393	21	.05*
444	13	.14*
477	17	.24
508	16	.08
542	16	.09
579	13	.04
613	12	.08
641	17	.09
678	29	.06
714	16	.07
835	25	.08
962	30	.12

*Poor signal/noise

**H. V. = 1090V, max anode signal 1.8×10^{-8} amp

RADIATION DAMAGE OF OPTICAL MATERIALS

An extensive program was undertaken at SBRC to identify radiation hardened optical materials for the Pioneer F/G IPP and Infrared Radiometer instrument. High energy electron (10 Mev) and 1-Mev gamma ray irradiation of filter glasses, silicone bonding agents, thin film coatings, crystals, and fiber optics was performed under this program. Transmission and reflection losses were measured as a function of accumulated dose and dose rates. The Hughes Aircraft Company linear accelerator facility and cobalt 60 sources were used to irradiate these materials.

A library of data on radiation damage to UV, VIS and IR optical materials as well as critical electronic components was accumulated as a function of exposure dose and dose rates. These data will be referred to in the selection of materials and components for this OPGT instrument. As an example of the value of this radiation data collected for the Pioneer project, it is expected that the total optical system of IPP will suffer less than 20% less in transmission after incurring an accumulated dose of 10^6 rad (Si) of electron bombardment during the Jovian fly-by. Similarly, this previous experience will provide a greater degree of confidence in the extrapolation of such data in defining an optical system for the OPGT instrument.

The major difference in emphasis for the present study is the inclusion of high energy protons (142 and 80 Mev) fluence of 5×10^{10} p/cm^2, at 6% duty cycle, and neutrons of similar fluences. Items so irradiated include six Hoya and six Schott color filter glasses covering a spectral range of 300 to 900 nm, germanium and silicon materials, MgF_2 and calcite crystals, Suprasil and Corning 7940 fused silicas, and a Polacoat 105 UV polarizer. Various silicone resins were also evaluated.

Proton and neutron bombardment caused, in general, less darkening than the equivalent fluence of either 10 Mev electrons or 1 Mev gamma rays. This is most likely because the stopping ranges were about 20g/cm^2 compared with 5g/cm^2 for 10-Mev electrons. It should be noted that the introduction of

actual hardware housings will in turn induce shower and bremsstrahlung radiation of smaller stopping ranges. Thus, damage in a finished instrument should be greater than indicated by these rudimentary tests of separate elements.

Table 4-4 gives some results for unshielded materials.

Table 4-4. Transmission Loss Due to 142 and 80 Mev Proton Irradiation

Color Filter Glasses		
Hoya	U330	30% loss $\lambda < 450$ nm
	LB130	<2% loss
	LB200	<1% loss
Schott	BG-23	<10% loss
	BG-24	16% loss $\lambda < 450$ nm
	WG-345	6% loss $\lambda < 550$ nm
	BG-12	10% loss $\lambda < 450$ nm
	R-62	<2% loss
	RG-715	No change
Crystals	MgF_2	<5% loss
	Calcite	Yellow tint
Polacoat	105 UV polarizer	No changes
Fused Silica		
	Corning C7940	<10% loss UV
	Suprasil	<10% loss UV
Silicone Resins		<5% loss UV
Thin Film Coatings		No measurable changes

MECHANICAL DESIGN

A list of approximate component weights appears in Table 4-5. The weights are based on the optical scheme shown in Figure 3-1. A similar exercise was conducted for an eight PMT instrument which provides simultaneous observation at four wavelengths. The total opto-mechanical weight was estimated at 6.50 pounds.

Table 4-5. Two PM Tube Type Instrument

	Weight (lb)
Aperture motor and sector	0.108
Filter and disc	0.132
Motor, filter disc drive	0.380
Primary mirror	0.058
Secondary mirror	0.014
Tubular case	0.850
Three bulkheads	0.150
Prism	0.206
PM tubes, 0.113 lb (two each)	0.226
Relay lenses, 0.011 lb (four each)	0.044
PM tube, relay lens, and prism holders	0.080
Secondary mirror spider	0.036
Miscellaneous parts	0.12
Total	2.40 lb

UV PASSBAND

The 270 nm passband (50 nm full width) is the most difficult to accommodate because of the spectral distribution from the planet and the dearth of filter materials. A calculation of the required out-of-band rejection was made:

Quantity	270 ± 25 nm	350 - 900 nm
Bandwidth, W	50 nm	550 nm
Solar irradiance, I	2.5×10^{-4} w/cm^5 nm	2×10^{-4} w/cm^2 nm
Geometric albedo Jupiter, p	0.28	0.45
Detector response	1	1
Transmission, T	T_u	T_v
Desired signal	100	<1

If it is required that

$$\frac{\text{Sig}_{(uv)}}{\text{Sig}_{(vis)}} = \frac{\int\left(p_u T_u I_u W_u\right)}{\int\left(p_v T_v I_v W_v\right)} \geqq 10^2,$$

then

$$\frac{\int T_u}{\int T_v} \geqq 10^2 \quad \frac{\int\left(I_v p_v W_v\right)}{\int\left(I_u p_u W_u\right)} \doteq 1.4 \times 10^4$$

Thus, for a leak < 1% when observing the disk of Jupiter with a GaAs detector, the required T_v value would be:

$$T_v \leq 7 \times 10^{-5}\, T_u.$$

It is possible to obtain an MDM filter with $T_{270\ nm} = 30\%$, and $T_{350\ -\ 900\ nm} = 3 \times 10^{-2}\%$. This is a factor of 14 greater than the required out-of-band response. Additionally, the use of a colored filter glass such as Corning 7-54 with the MDM filter will assure that the required rejection can be achieved. However, the transmittance of this filter glass is reduced when irradiated with high energy particles or gamma rays. A mission requirement for operation in radiation environment therefore may preclude the use of this compound configuration.

Section 5
DETECTOR SURVEY AND TRADE-OFF STUDY

As stated earlier, the detector selection study was heavily weighted toward the evaluation of a specific PMT. However, in the event that instrument requirements are changed at some future time, it may well be desirable to reconsider the detector selection. For the sake of completeness, therefore, a brief synopsis of selected pertinent factors are given here for several candidate detectors which fail to satisfy the present set of OPGT photometer-polarimeter requirements for one reason or another.

It is beyond the scope of this report to cover all detector possibilities in detail. The intent rather is to survey the state of the art for several common types of detectors and perform a trade-off comparison study. Available literature related to PMTs and solid-state detectors was used for obtaining pertinent data for this report. Pioneer F/G channeltron test data were extracted for inclusion here.

CHANNELTRONS

Channeltron photomultiplier detectors were used in the Pioneer IPP instrument. These devices are extremely quiet in terms of dark noise, operate over a wide dynamic range of gain, and are quite stable and linear. The channel multiplier is a continuous dynode and requires no dynode resistor-divider nor the attendant power loss as do conventional PMTs. They are available in many configurations with a variety of photocathode response characteristics, and are small and lightweight.

Channeltrons, because they utilize a thin-film solid-state electron multiplier, exhibit a finite life span. Experience has shown that after approximately 1-coulomb of charge has passed through the anode of a channeltron, the gain will have degraded significantly. Thus, for applications such as polarimetry where large anode currents are necessary to achieve a high SNR

to achieve the required precision, the detector life will be short. This, of course, is a significant detriment for a long duration mission. Moreover, even under conditions of expected long term low-level operation, an accidental exposure of these devices to high ambient illumination could render them useless early in the mission.

Although they are extremely high gain devices, channel-multipliers must be limited in output current to a maximum of approximately 10^{-7} amp. Normally, this is not a serious limitation because the dark current is very small, on the order of 10^{-17} to 10^{-18} amp referred to the photocathode. However, when operating at temperatures above 50°F or in a radiation environment, the dark current will rise significantly. Therefore, the margin between dark current level and maximum anode current becomes more limited in dynamic range as the environment becomes more hostile. Note in Figure 5-1 that when operating at a channel voltage of 1.5 kv (typical of IPP in polarimetry mode) in a radiation environment of 10^3 rad (Si) per hour (Jovian belt levels at 3-4 R_j) only 1-1/2 decades of dynamic range remain. A device capable of larger output currents would therefore be desirable for applications where a high SNR is imperative for necessary precision.

Figure 5-2 shows three curves for a channeltron operated at 10^3 rad/hr with illumination. The lower curve illustrates the component of dark current due to electron interaction with the channel multiplier only; the middle curve shows the additional dark contribution of the combined photocathode, glass scintillation, Cerenkov radiation, etc.; and the upper curve shows the output current for a specific illumination level which produces 10^{-10} amp at 1.5 kv under a nonradiation environment. Note that this value is raised to saturation above the 10^{-7} limit when subjected to 10^3 rad/hr.

Curves shown in Figures 5-1 and 5-2 were extracted from previous Pioneer F/G work. Figure 5-3 is presented as an indication of the gain spread of a number of channeltrons fabricated for the IPP. Figure 5-4 indicates the effect of temperature on dark current for a typical channeltron with

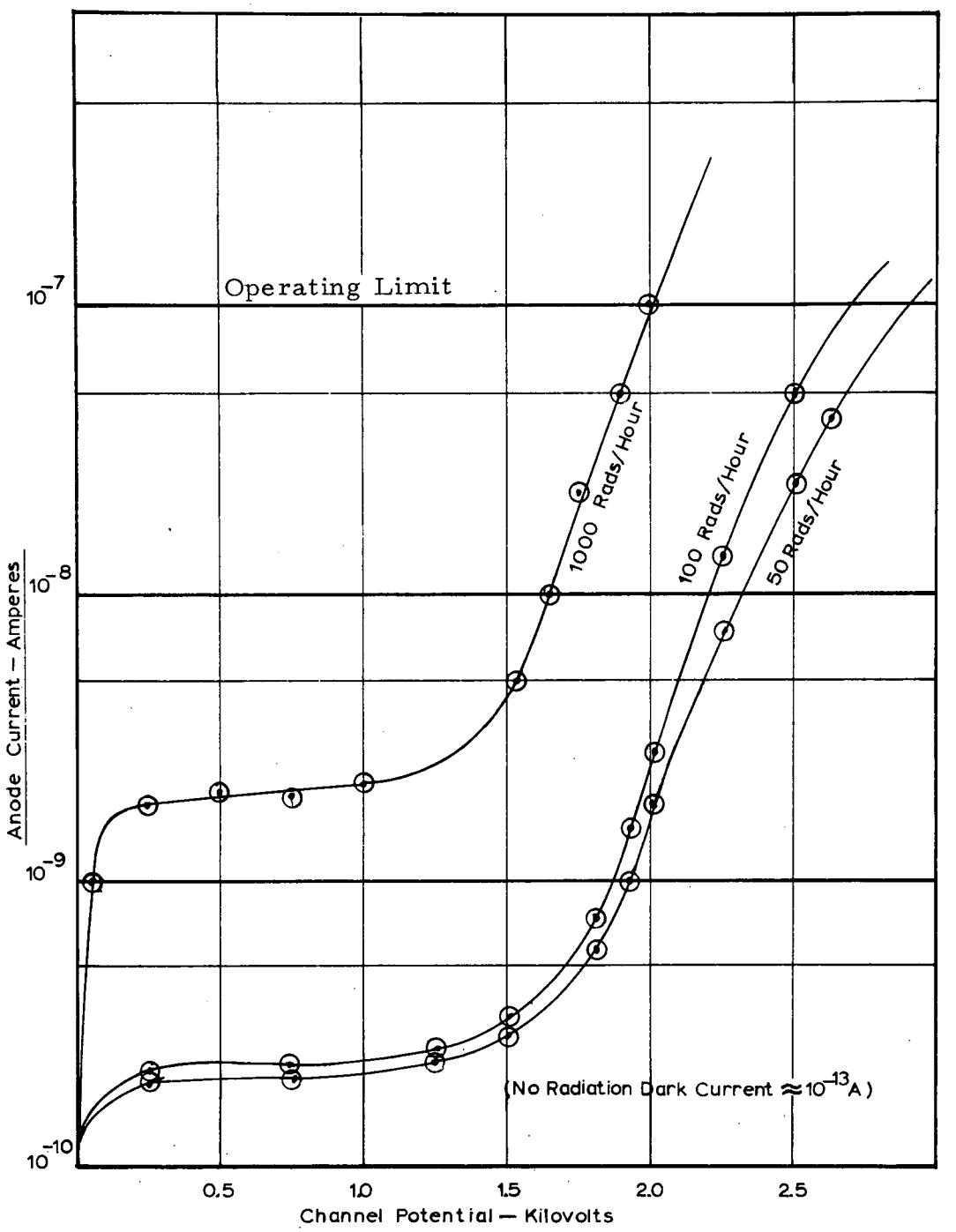

Figure 5-1. Channeltron Anode Current as a Function of Channel Potential when Exposed to a Radiation Environment

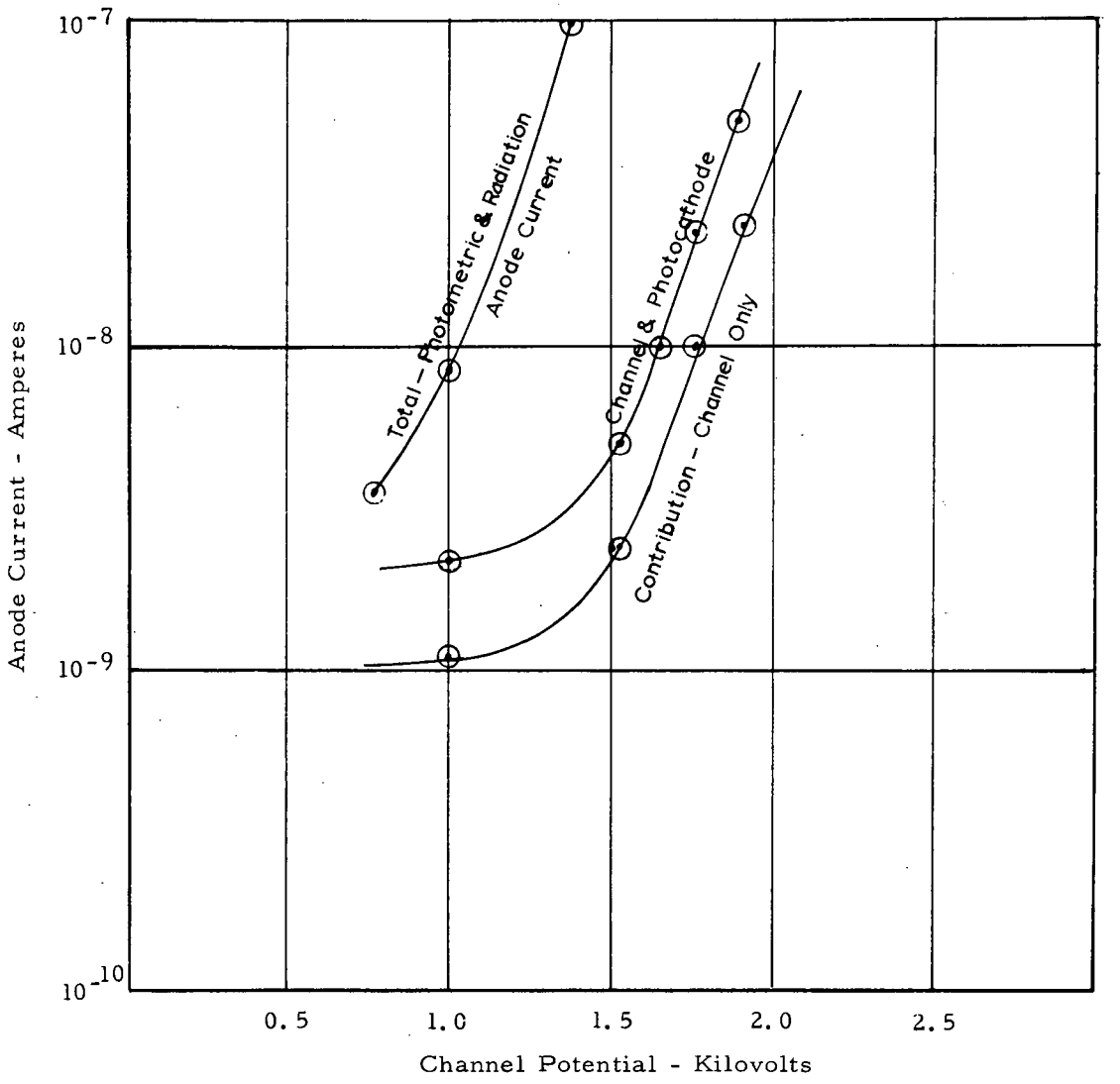

Figure 5-2. Effect of Simulated Jovian Trapped Radiation Belt Environment on Channeltron Anode Current Illustrating Contribution of Electron Interaction with Channel Multiplier, Photocathode, and Glass Envelope (Cerenkov Effect)
Dose = Approximately 10^{-3} rad/hour

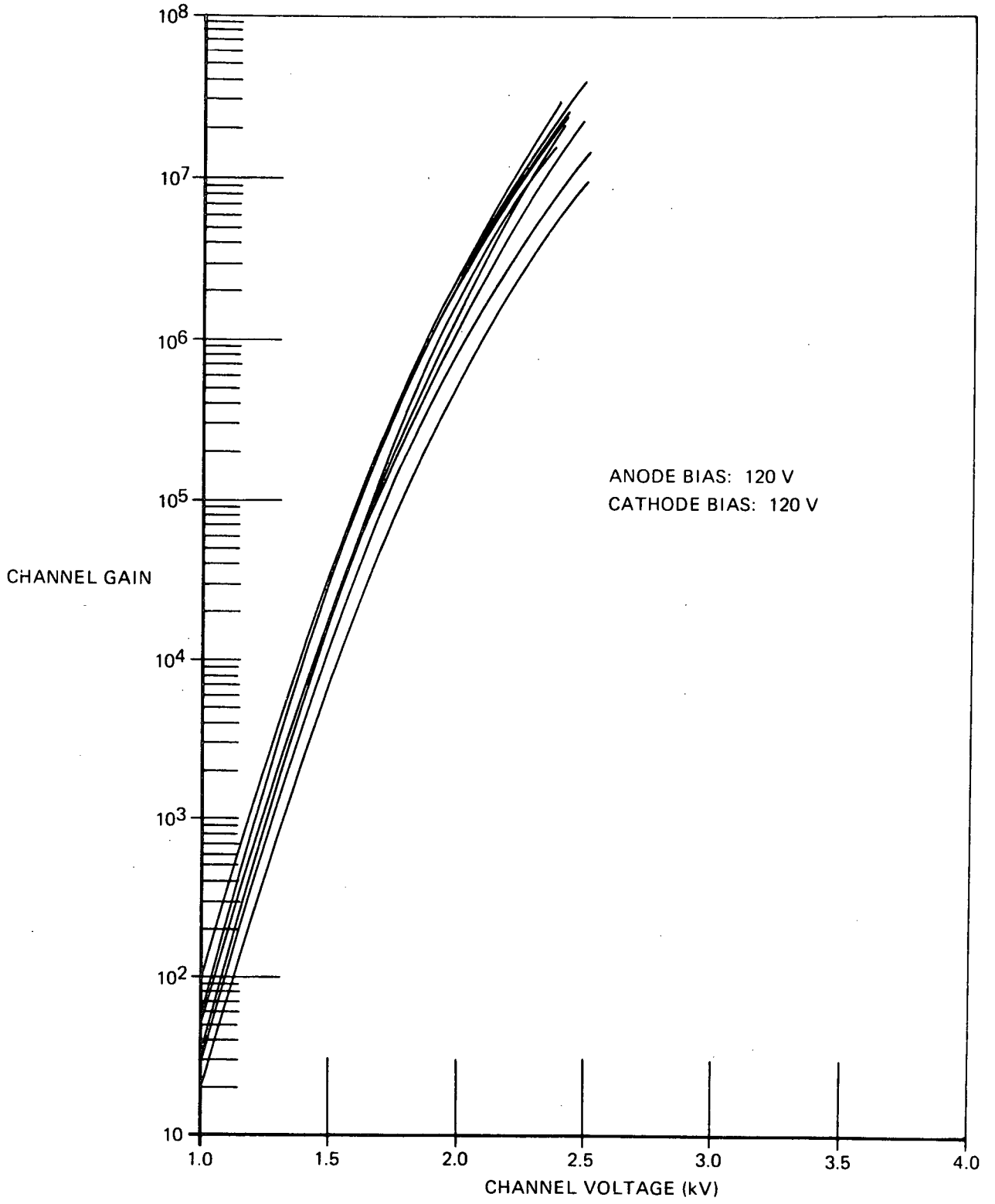

Figure 5-3. Typical Electron Gain Characteristics of Channeltron Multipliers in BX 784 Tube

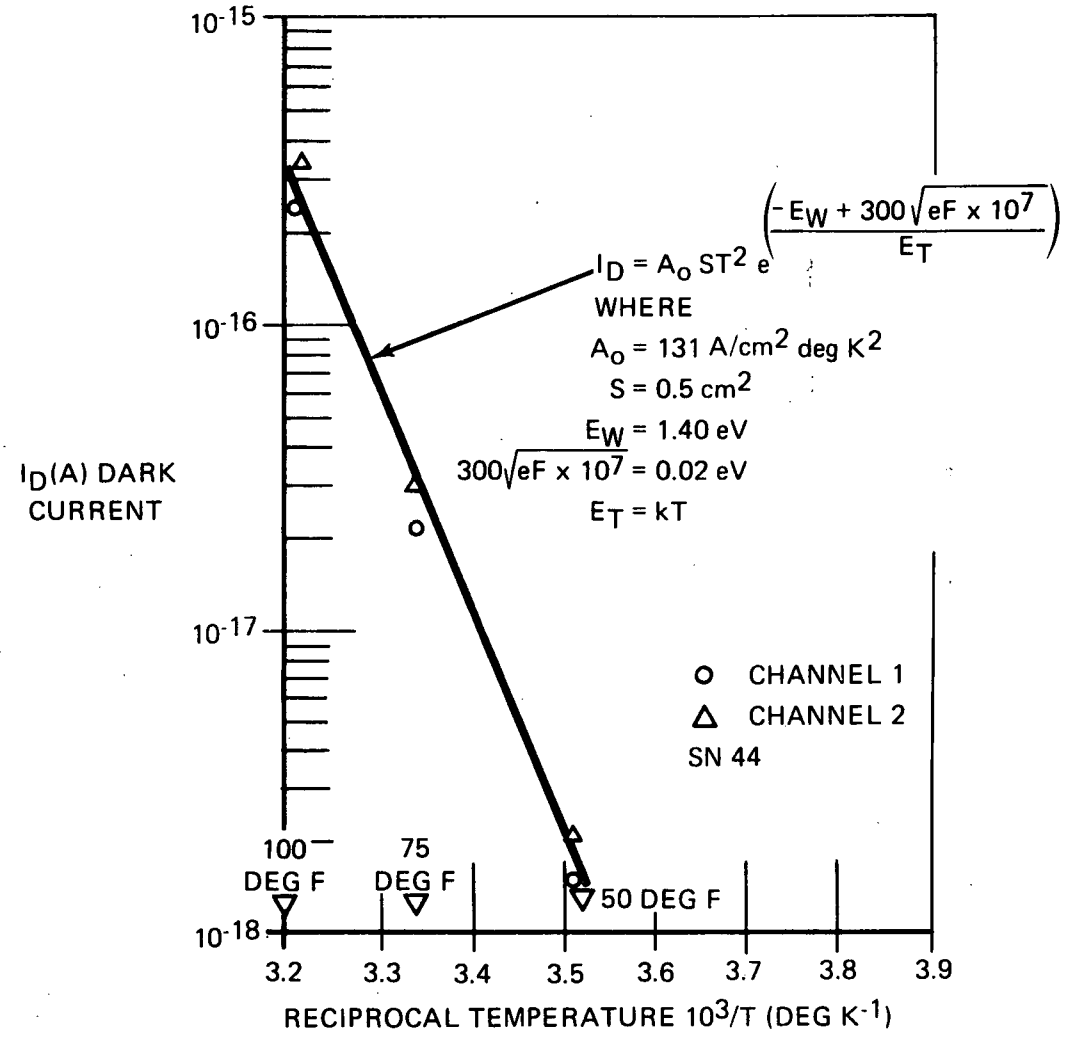

Figure 5-4. Dark Current vs Temperature for Dual Channeltron with S-20 Cathodes

an extended-Red S-20 type photocathode. These data presumably will apply to any device using a similar photocathode (PMTs, photodiodes, etc.).

In summary then, the channeltron is a useful device for low current and limited life applications where high sensitivity and wide dynamic range are required. It requires a high-voltage power supply, which can be inherently smaller and simpler than the equivalent for a PMT. However, inclusion of this HVPS requirement implies a size/weight/power impact. The ability to count individual photons makes the channeltron especially attractive for low light level applications. For high level photometry/polarimetry, however, where a high SNR is necessary, this count rate becomes too excessive for practical use (GHz ranges).

SOLID STATE PHOTODETECTORS

A wide variety of photosensors has been compounded from semiconductor materials for various applications. Basically such photodetectors exhibit very high quantum efficiencies (>75% typically) but suffer from leakage current noise which establishes a threshold noise-equivalent-power (NEP) at low illumination levels. For applications where high flux levels are available (photon noise-limited cases) solid-state detectors become the obvious choice because of their small size, inherent ruggedness, stability, insensitivity to overloads, uniformity of response, and minimal power supply requirements. Moreover, unlike PMTs and channeltrons, semiconductor detectors can be fabricated in a wide variety of sizes and shapes which can be an advantage in many optical systems.

Multielement compounds have been produced which exhibit quantum efficiencies approaching unity (HgCdTe, PbSnTe, InSb, InAs, etc.). Generally, detectors made of these materials cover a broad spectral range extending far into the infrared region. Such response would be a detriment to this OPGT application since special techniques would be necessary to eliminate the noise resultant from this unused and unwanted spectral response. Also, significant cooling of these detectors is normally required; e.g., to 77°K for

an InSb detector with a 5.5-μm long wavelength cutoff. If, however, the spectral range of some future instrument is extended into the infrared region, and zodiacal (or other low level) light measurement is not required, then such solid state devices could become prime detector candidates.

Over the past decade a considerable amount of technical progress has been made in the development of silicon photosensors to operate in the visible spectrum. Of those available (phototransistors, photo-FETs, and other like devices) the silicon photodiode appears at this time to have attained the highest degree of development. Many of these devices, particularly a PIN diode in combination with a high-gain monolithic operational amplifier, can outperform a typical PMT in situations where very low light levels and the spectral region shortward of below 400 nm are not of concern.

Of the three basic types of silicon photodiodes diffused P on N, diffused N on P, and Schottky barrier, the latter would seem most suitable for the photometer-polarimeter instrument because of its enhanced UV response. Since the detectors required for the OPGT instrument are individual units and thus may be physically isolated rather than combined in the more common array configurations, special fabrication techniques may be used. For example, providing a guard ring and incorporating an intrinsic region in the junction area could be used to enhance performance and to shape the spectral response of these devices to a specific application.

Figure 5-5 shows the reduction in dark current achieved with the addition of a guard ring. (Also note that for very small area detectors, <0.1 cm^2, the planar diffused devices exhibit low dark current properties.) The addition of the intrinsic region (PIN configuration) will improve response time, responsivity, and most importantly, it will improve the linearity at high light levels.[7]

Figure 5-6 shows the relative spectral response of typical silicon detectors. The UV enhanced (dotted) curve indicates that the response is extended down to below 200 nm. The enhancement in this spectral region is

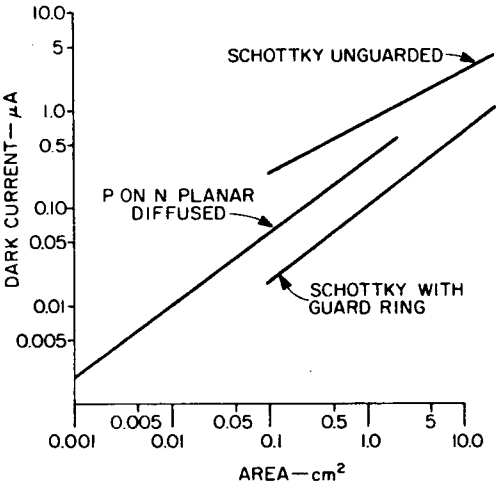

Figure 5-5. Typical Total Dark Leakage Current vs Active Area for Silicon Photodiodes, All Fabricated on 1000 ohm cm silicon Material

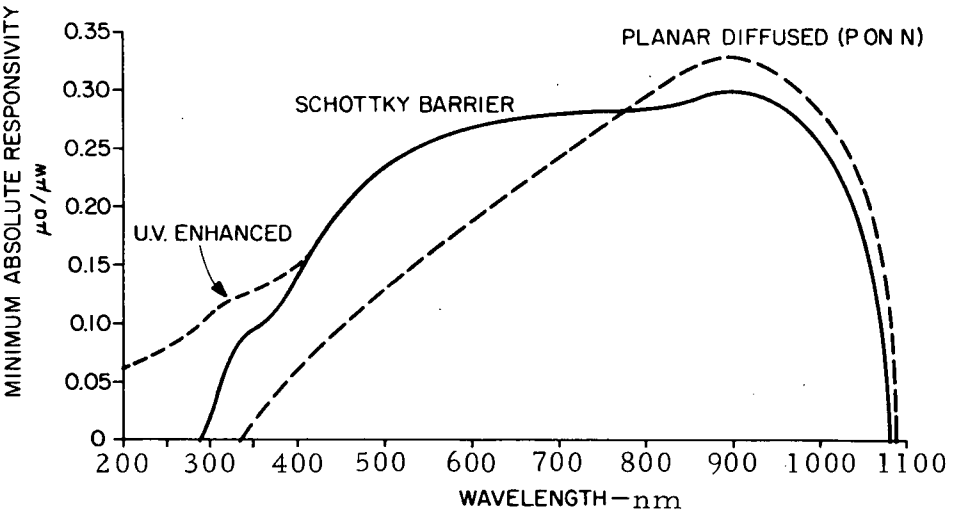

Figure 5-6. Spectral Response for PIN Photodiodes (From United Detector Technology Brochure)

accomplished with antireflection coatings.[8] Response beyond 950 nm is affected by the thickness of the base material and depletion depth.[9]

Although these physical factors may be varied to shape the overall device responsivity, it is readily noted that solid-state detectors are, in general, deficient in blue response below 400 nm. However, if the required instrument response in the blue region were relaxed, a Schottky barrier detector should be considered for this application (again assuming no zodiacal light).

Typical parameters are: NEP of 2×10^{-13} watt/$Hz^{\frac{1}{2}}$ at 1000 Hz chopping frequency on a 1-cm diameter detector; half-power spectral response from 400 to 1020 nm, dark leakage current of 3×10^{-8} amp at 10 volts bias.[10] Response time of semiconductor diodes is in general very fast (ns) and need not be considered a problem for the OPGT instrument requirements.

The latest available radiation susceptibility data indicate that semiconductor photosensors are no more vulnerable to radiation damage than other detectors.[11] In fact, because the active area can present a small cross section, and because no window material need be used, the solid-state detector may be even less vulnerable to radiation damage than equivalent PMTs. Data indicate that light to moderate damage occurs at proton fluences of 10^{12} or 10^{13} P/cm^2 (E_p = 15 MeV) with serious damage occurring at 10^{17} P/cm^2 for typical silicon photodiodes.

Effects of electron bombardment are equally encouraging. Data indicate that degradation begins with an accumulative dose of 10^6 rad with serious damage occurring at 10^7 to 10^8 rad.[12]

PHOTOMULTIPLIER TUBES

Operational behavior of the PMT is well known and many parameters of a wide variety of tube configurations have been abundantly documented. These devices have been used as the primary detector in virtually all precision photometric instruments for many years. There is no question therefore, that mission objectives of the OPGT photometry/polarimetry team could be

accomplished with a high probability of success through the use of appropriate PMTs.

Although evolution of the PMT has progressed to a high degree of sophistication, a number of undesirable attributes remain, such as: the requirement for high voltage at sufficient power to supply the dynode resistor-divider; large size, relatively bulky package, nonuniform cathode sensitivity, fatigue when exposed to overloads, existence of secondary time constants, temperature sensitivity, and loss of sensitivity with time (long term drift). Many of these undesirable aspects result from the photocathode, and thus exist to varying degrees depending on the specific mix of alkaline salts used in the photocathode formation.

RCA has recently developed a line of PMTs using a new photocathode concept. These devices use cleaved crystals of Type 3-5 semiconductor compounds in place of conventional alkali-salts as a photosensing medium. One such crystal, GaAs, combined with a conventional electron-multiplier dynode structure, yields a PMT with outstanding properties. Responsivity is relatively constant at 100 ma/watt (cathode) from 180 nm (depending on window material) to 900 nm, with a sharp cutoff at 910 nm. Many of the deficiencies attributed to the common "S" type photocathodes do not exist with the cleaved crystal type. Thus, this new device appears to promise superior performance in addition to eliminating the need for several PMTs to cover the desired spectral range.

Before turning attention to the evaluation of this new device, however, a review of radiation damage literature pertinent to conventional PMTs was conducted. Many investigations have produced data depicting the radiation effects on conventional PMTs. Therefore, sufficient data are available from which to establish a comparative baseline for evaluation of the new GaAs type device.

In general, PMTs have exhibited no degradation for accumulated dosages up to 10^4 rad, but begin to exhibit reduced responsivity between 10^5 to 10^6 rad.

Typically, degradations of 20% to 30% are commonly experienced after 10^6 rad cumulative exposure. This, of course, is dependent on the window material. Data shown in Table 5-1 are typical for space-quality PMTs (EMR Type 541).* These data were obtained at the Hughes Aircraft Company, Radiation Laboratory, using a ^{60}Co source. The difference in 7056 glass windows and sapphire is readily apparent. Exposure of these tubes was done at relatively high fluence rates, thus one may question that this effect may differ at other flux rates.

Other investigations have studied the effects of earth orbit conditions on typical EMR type PMTs. One such investigation combined long term exposure to electron and proton bombardment simulating the earth's Van Allen belt flux levels, and included illumination levels which simulated solar radiation, moon and earth albedo.[13] After a test period of 4552 hours, the tubes had degraded as shown in Table 5-2. Obviously, these data indicate less degradation than a cumulative exposure of 10^6 rad. However, it is interesting to note that degradation occurs mainly where radiation exposure is combined with illumination; i. e., in operation.

Table 5-1. Accumulated Dose Experiments on EMR Photomultiplier Tubes (^{60}Co Source at Hughes-Fullerton)

Tube Type →	541E-01-14 (S-20, 7056 Glass)		541E-05-14 (S-20, Sapphire)		541A-01-14 (S-11, 7056 Glass)		541A-05-14 (S-11, Sapphire)	
Dose	I_{light}†	I_{dark}	I_{light}†	I_{dark}	I_{light}†	I_{dark}	I_{light}†	I_{dark}
Negligible (Baseline)	1.35×10^{-8}	1.3×10^{-11}	3.75×10^{-8}	---	4.1×10^{-8}	---	6.4×10^{-8}	1×10^{-10}
After 10^4 rad	1.35×10^{-8}	8.0×10^{-10}	3.3×10^{-8}	1.1×10^{-9}	4.4×10^{-8}	6.2×10^{-10}	6.0×10^{-8}	6.2×10^{-10}
After 10^5 rad	1.55×10^{-8}	4.4×10^{-9}	3.6×10^{-8}	1.1×10^{-8}	4.4×10^{-8}	4.8×10^{-9}	6.2×10^{-8}	2.3×10^{-9}
After 10^6 rad	1.55×10^{-8}	5.7×10^{-9}	3.5×10^{-8}	4.0×10^{-8}	3.3×10^{-8}	5×10^{-9}	6.1×10^{-8}	4.4×10^{-9}
Retest	1.05×10^{-8}	9.0×10^{-11}	3.2×10^{-8}	1.9×10^{-10}	2.75×10^{-8}	1.2×10^{-11}	6.35×10^{-8}	6.0×10^{-11}

†Using gallium phosphide diode light source at 100 ma and 1000 volts across the photomultiplier.

*EMR: Electro Mechanical Research Company.

Table 5-2. Degradation of EMR 541 Series Multiplier Phototubes Exposed to Radiation

Exposure	Tube Serial No.	% Change Voltage for 10^6 Gain	% Change QE at 399 nm	% Change QE at 500 nm
Electrons and Protons	11644	~0.3	+4.9	+6.5
Electrons, Protons, Earth Albedo	11762	+2.5	-9.8	-8.7
Electrons, Protons, Earth Albedo, Lunar Illumination	11647	+8.6	-7.4	-13.5
Earth Albedo	11664	-0.6	+12.6	+25

GaAs PHOTOMULTIPLIER

Because PMTs equipped with GaAs and GaAsP photocathodes offer the best prospect of meeting all OPGT photometry/polarimetry team objectives, a considerable effort was allocated to evaluate this new device. Specifically an RCA 31025J PMT was procured for evaluation. This tube was selected because it is identical in structure to the extremely common 931 and 1P21 tubes for which more than 20 years of data are available. Although the tube geometry is not as useful as other available devices, it was felt that attributes of the new photocathode could more readily be separated from a device where the electron multiplier section was well established.

The RCA C31025J PMT was selected with a sapphire window rather than with the standard 7056 glass envelope. This selection allows full evaluation of the GaAs photocathode into the UV spectral region with virtually no influence from the window. It is recognized that sapphire scintillates and fluoresces under the effects of a radiation environment. However, these effects can be related to previous test data and can be compensated accordingly.

Sapphire has exhibited excellent nondarkening properties as a function of radiation dose, and thus should not enter as a source of error in the evaluation of photocathode degradation measurements.

Recognizing that, statistically, one sample is not necessarily representative of the generic class, the 31025J tube was evaluated, and typical performance data are presented in the following section. In general, the tube behaved as advertised and therefore has been included as part of the SBRC recommended instrument design.

Section 6
GALLIUM ARSENIDE PHOTOMULTIPLIER TESTING

As a result of the combination of requirements for the planetary and zodiacal light measurements, an RCA C31025J photomultiplier with a GaAs photocathode was selected as the best off-the-shelf detector for the photometer-polarimeter. An extensive series of tests were run on this detector to assure its suitability for such an application. Measurements of the relative spectral and polarimetric responsivities were included in the optical component test results.

In Figure 6-1 the percent change of anode current as a function of time from initial turn-on is shown. For this test, the flux level was adjusted to yield an initial anode current of 1.0 μa for a high voltage (cathode to anode) of 900 volts. After an approximately 6% drop in overall responsivity during the first 80 hours, the output current stabilized and remained constant for the remainder of the test. All anode current measurements were performed with a Keithley Instruments Model 410A Picoammeter.

The differential current gain as a function of high voltage was measured in the 1000 to 1200 volt range. A decade gain change required about 360 volts for this tube. Figures 6-2 through 6-4 show tube linearity measurements over three decades for flux centered at 400, 550, and 700 nm. A high voltage of 1200 volts was used for the 400 nm data and 900 volts for the longer wavelengths.

The angular responsivity of the RCA C31025J photomultiplier is shown in Figure 6-5. An SBRC collimator and associated source provided the fixed geometry, small angular divergence flux input for this test. The detector was mounted on a rotatable table with the tube and table axes concentric. The angle of incidence then was varied with the rotatable table.

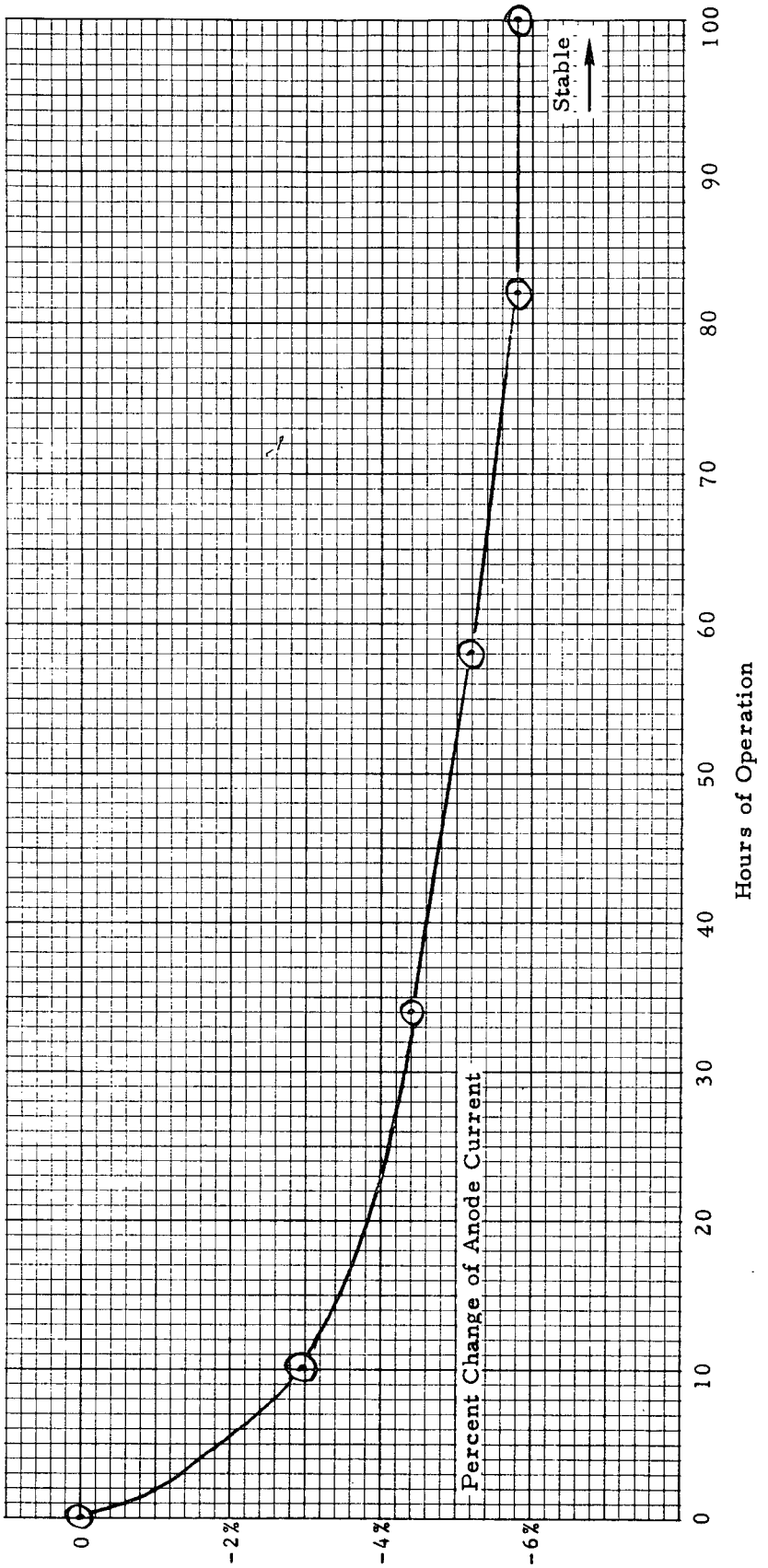

Figure 6-1. Life Test of GaAs Photomultiplier Tube (RCA C31025J). Percent Change of Anode Current (1 μa initial value) as a Function of Time from Initial Turn On for Constant Flux Input.

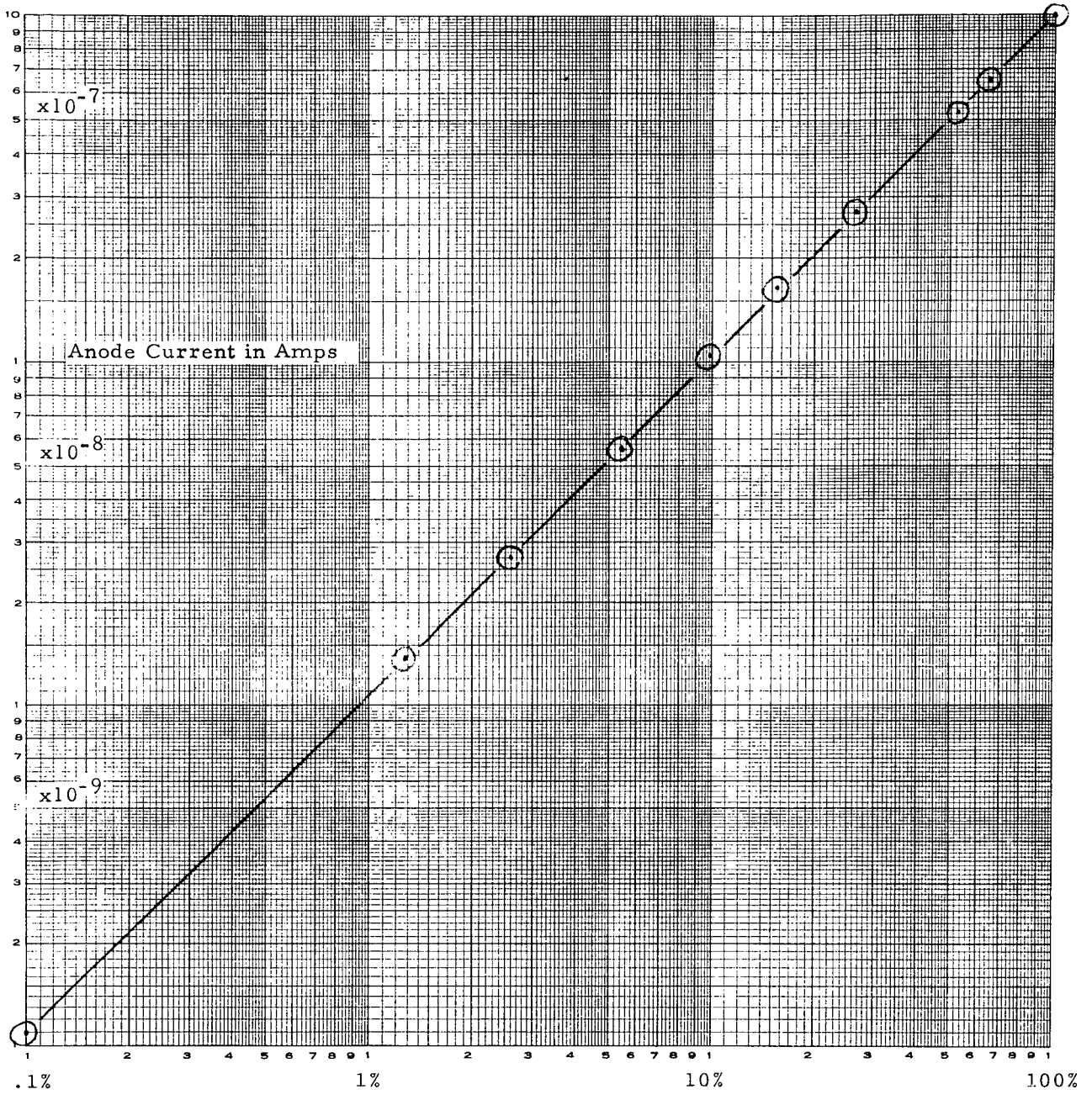

Figure 6-2. Linearity Test of GaAs Photomultiplier Tube (RCA C31025J) Anode Current vs Neutral Density Filter Transmittance with Incident Flux Near 400 nm

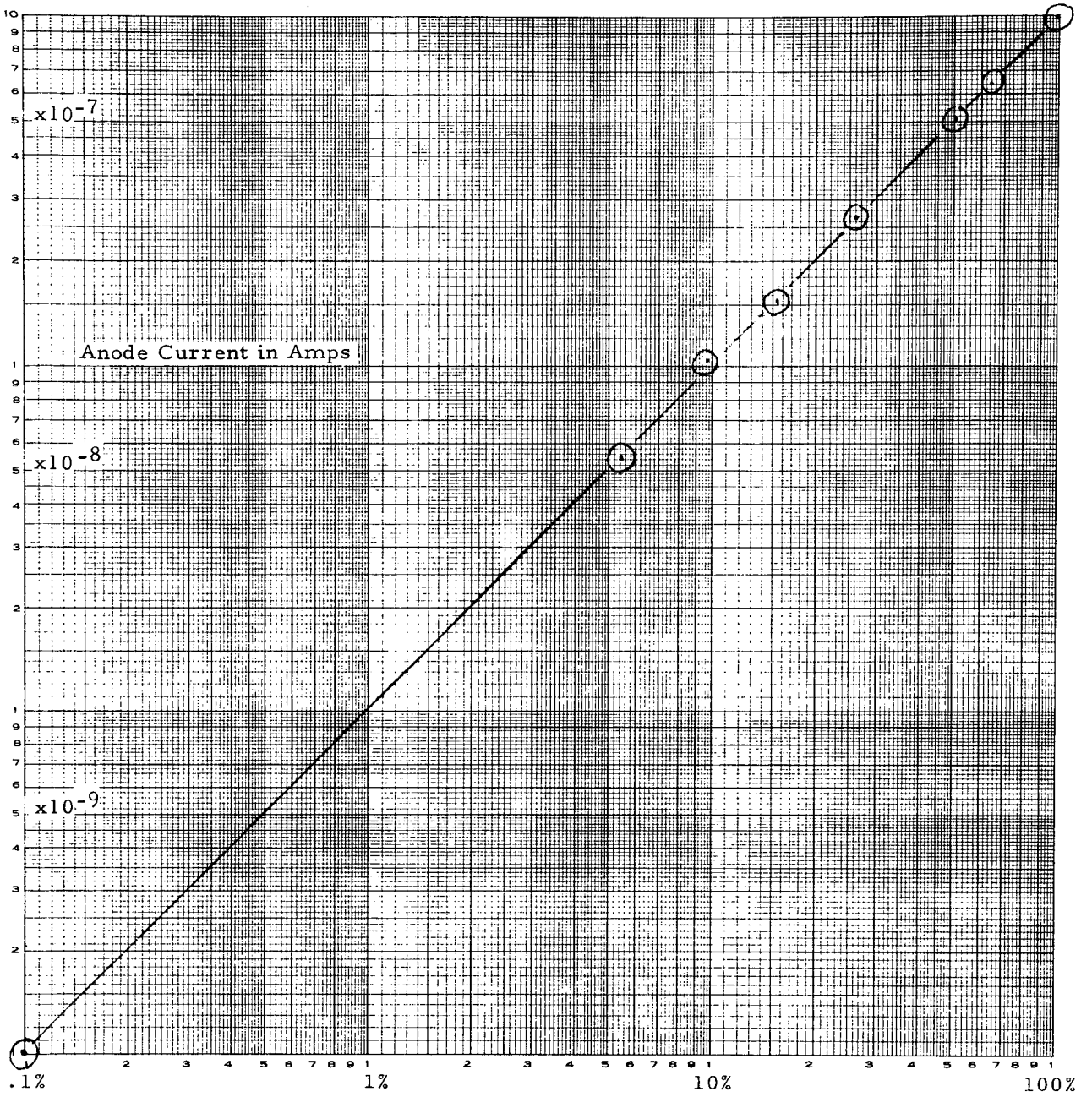

Figure 6-3. Linearity Test of GaAs Photomultiplier Tube (RCA C31025J) Anode Current vs Neutral Density Filter Transmittance with Incident Flux Near 550 nm

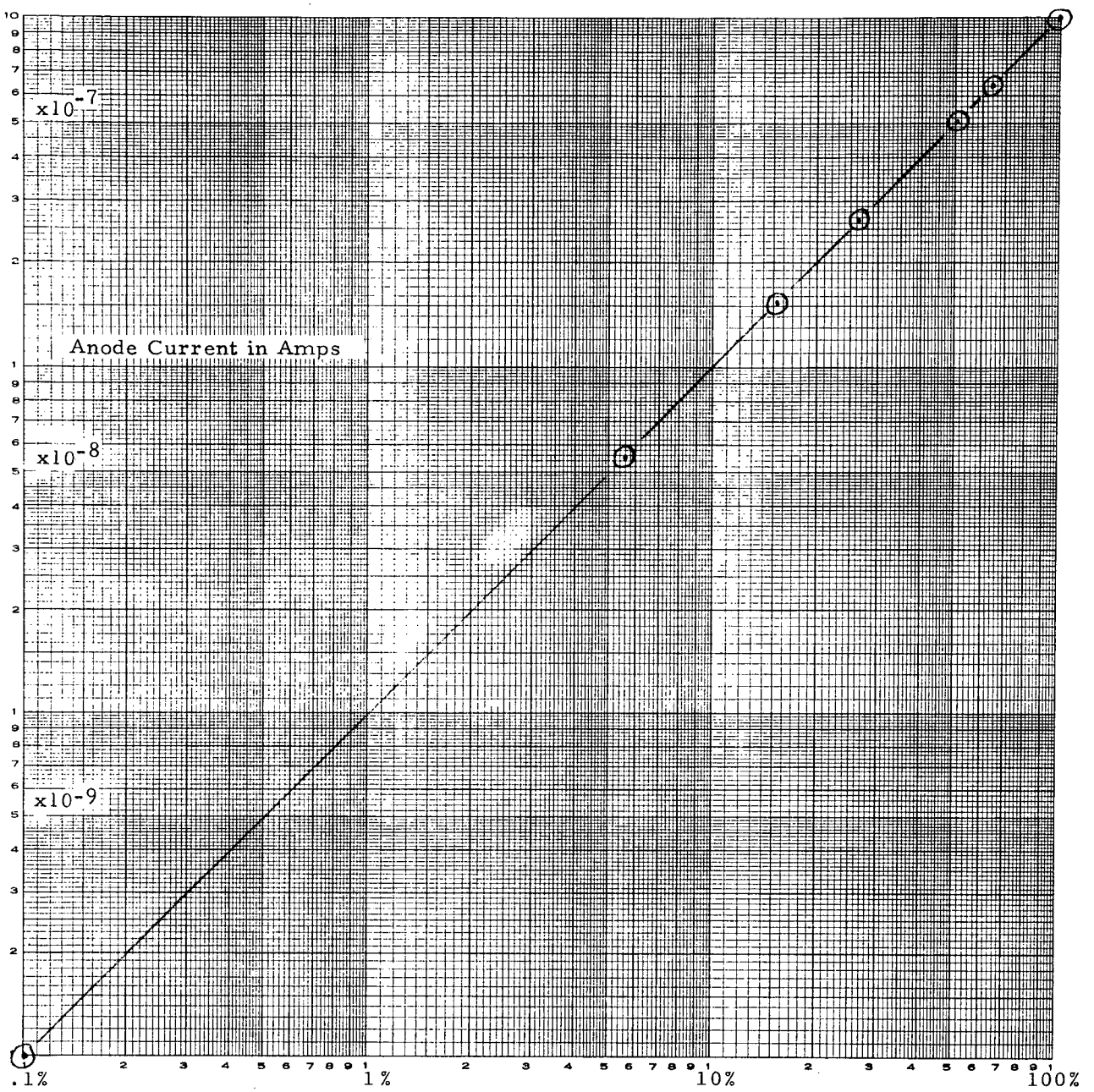

Figure 6-4. Linearity Test of GaAs Photomultiplier Tube (RCA C31025J) Anode Current vs Neutral Density Filter Transmittance with Incident Flux Near 700 nm

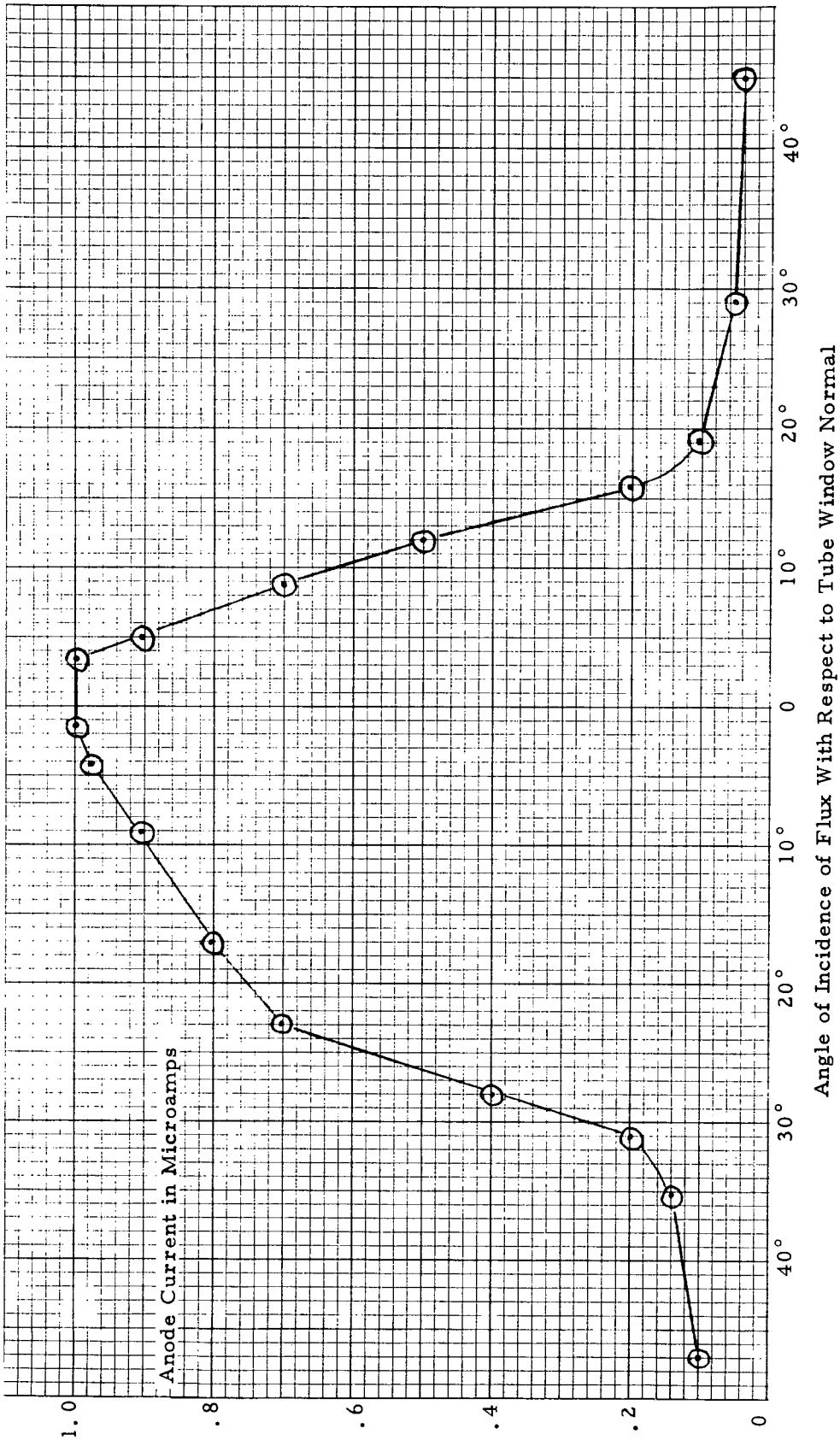

Figure 6-5. Angular Responsivity of GaAs Photomultiplier Tube (RCA C31025J). Anode Current Versus Angle of Incidence of Flux at Tube Window.

Figure 6-6 shows the results of spot scans taken across the photocathode (in a direction perpendicular to the tube axis of symmetry). Cross scans were taken 25 mils towards the tube base and 75 mils towards the top from the cathode center. Because of the grid wires located in front of the photocathode there was a variable obscuration as the cross scans were made which probably accounts for the slope differences in the three cases. Figures 6-7 through 6-9 show similar scans run parallel to the tube axis of symmetry that pass through and ±50 mils from the photocathode center. The modulation caused by the grid wires is clearly seen in these scans and thus do not lead to an interpretation problem as with the cross-scan data.

Cobalt-60 sources were used to subject the C31025J to electron and gamma ray bombardment. Two types of measurements were made with the tube active in the radiation environment: dark current was measured as a function of high voltage while subjected to dose rates from approximately 10 rad (Si)/hour to approximately 40 rad/hour; secondly, anode current was measured as a function of illumination level while subjected to the same radiation doses, but at two different high-voltage (gain) settings. Graphs of the resultant data are shown in Figures 6-10 and 6-11 respectively. Finally, the dark current and anode current resulting from an arbitrary illumination level was plotted as a function of time before and after subjecting the tube to a 7000-curie cobalt-60 source (inactive) yielding a cumulative dose of 10^6 rad in 70 minutes (see Figure 6-12). Post exposure dark current is excessively elevated due to the combined radiation effects, however much of this is probably attributable to the sapphire window. Generally the tube degraded $\approx$ 12% and the dark current was increased in excess of an order of magnitude permanently.

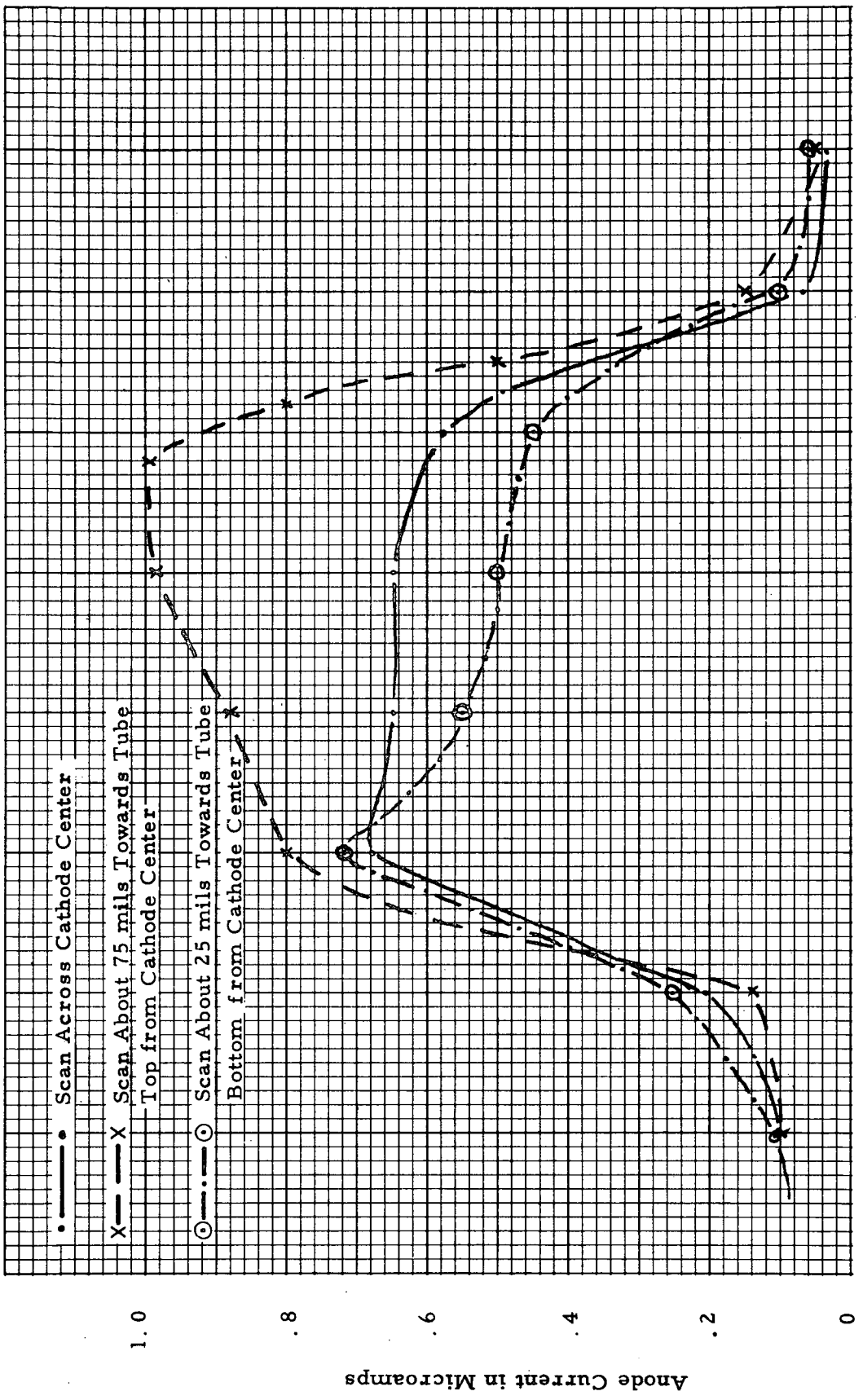

Figure 6-6. Spot Scan of GaAs Photomultiplier Tube (RCA C31025J). Anode Current Versus Horizontal Spot Displacement Across Three Different Portions of Cathode.

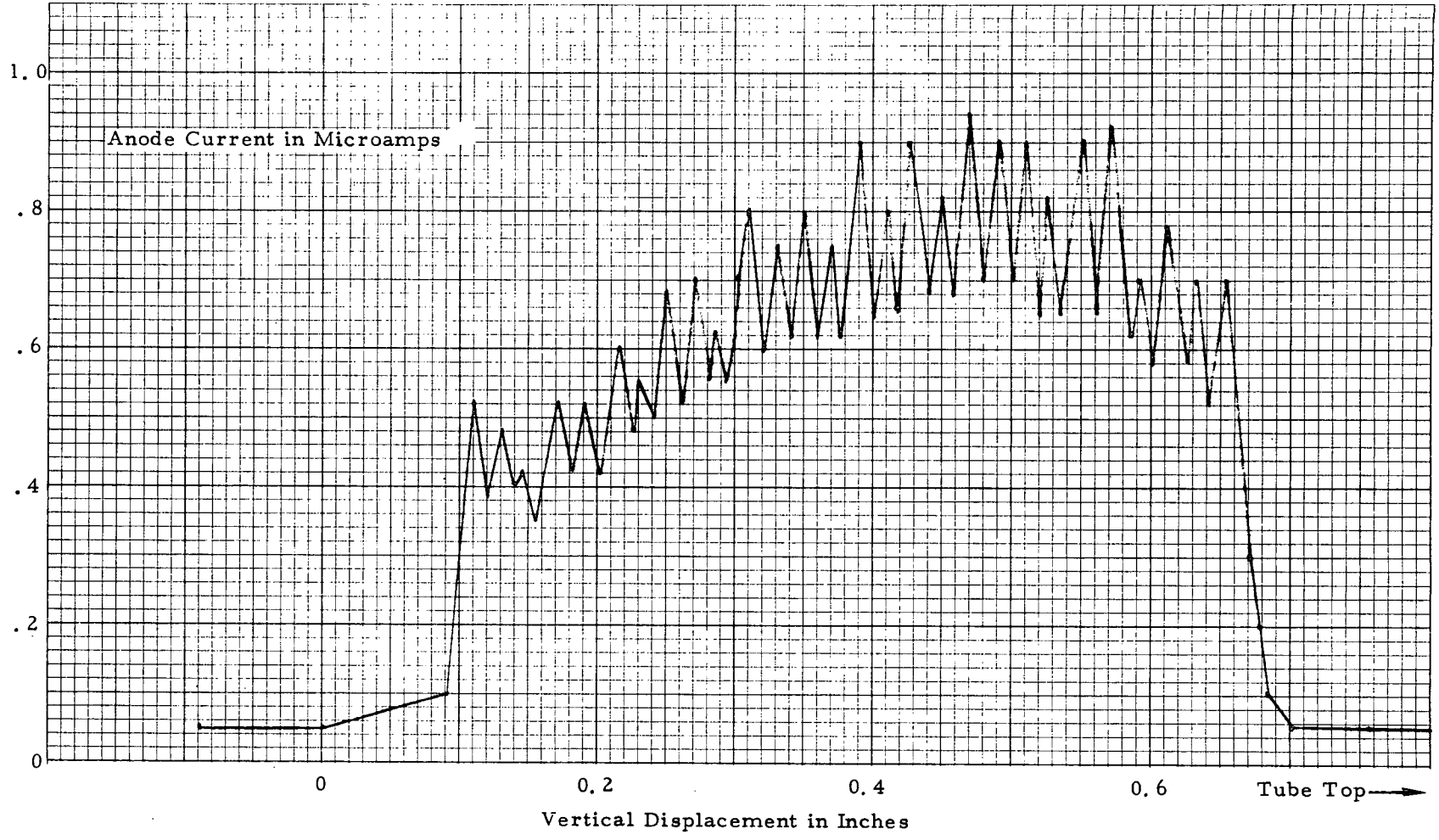

Figure 6-7. Small Spot Scan of GaAs Photomultiplier Tube (RCA C31025J). Anode Current Versus Vertical Spot Displacement Along Photocathode Center Line. (Modulation produced by Grid Wires in Front of Photocathode.)

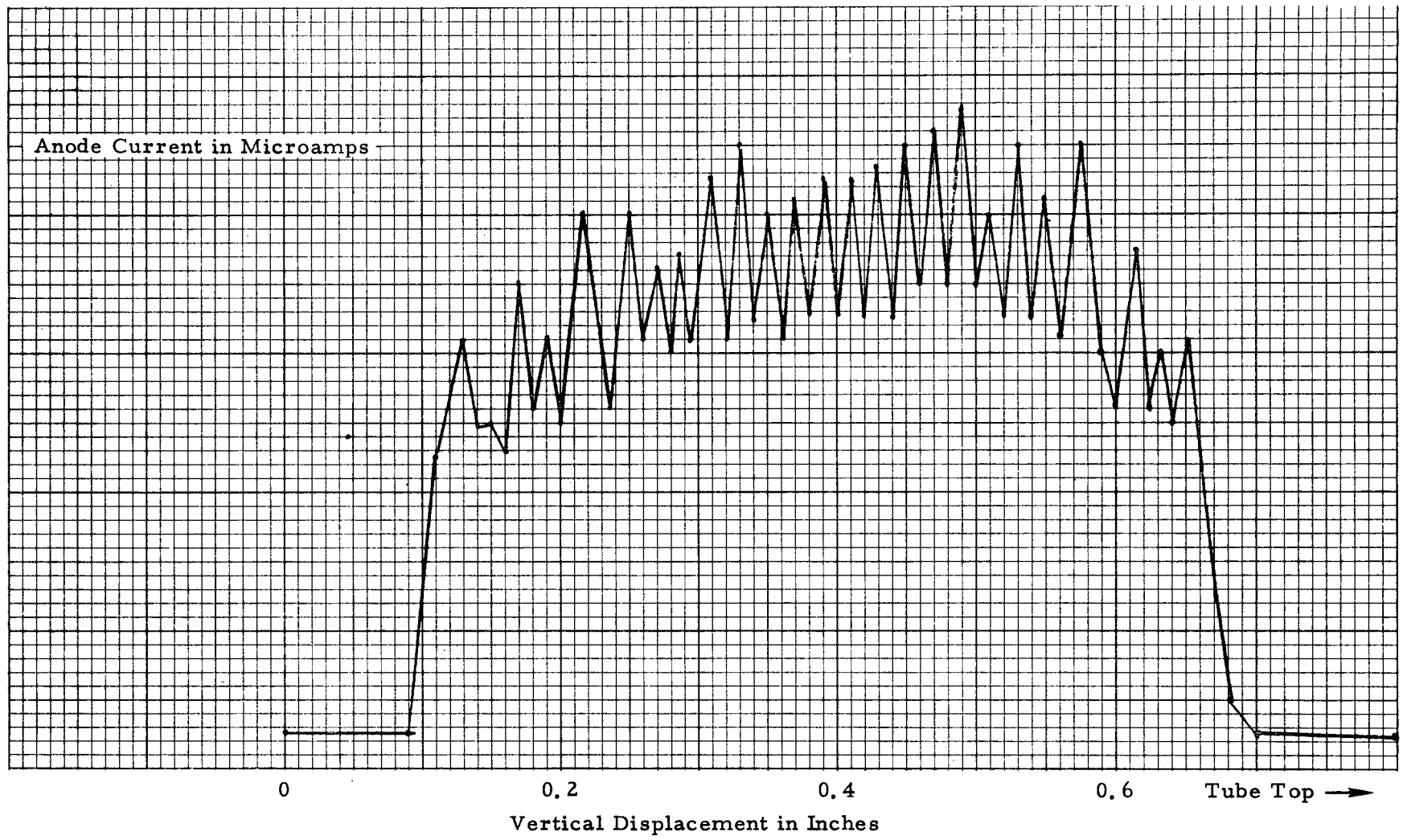

Figure 6-8. Small Spot Scan of GaAs Photomultiplier Tube (RCA C31025J) Anode Current Versus Vertical Spot Displacement 50 mils to Left of Photocathode Center Line. (Modulation Produced by Grid Wires in Front of Photocathode.)

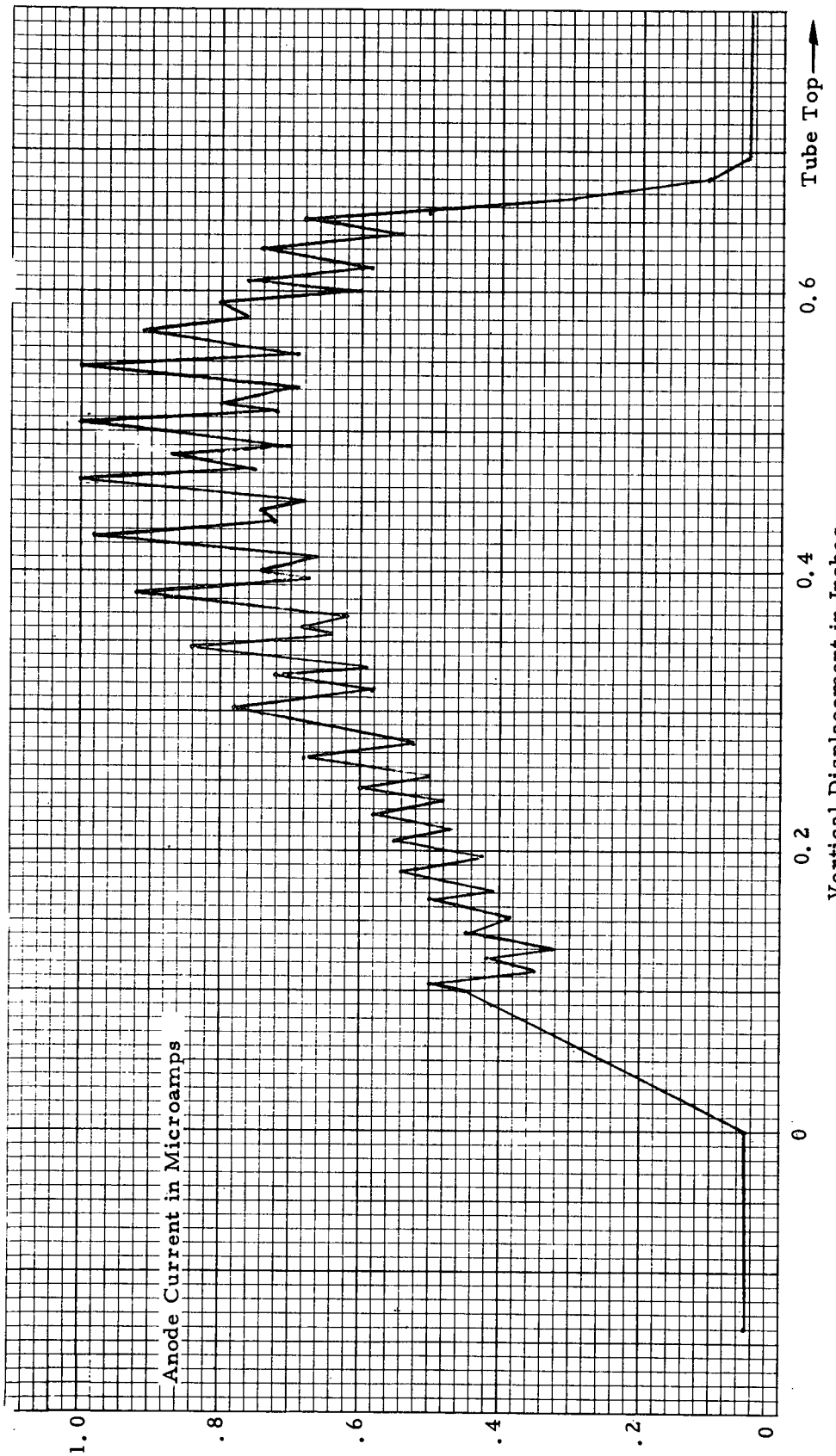

Figure 6-9. Small Spot Scan of GaAs Photomultiplier Tube (RCA C1025J). Anode Current Versus Vertical Spot Displacement 50 mils to Right of Photocathode Center Line. (Modulation Produced by Grid Wires in Front of Photocathode.)

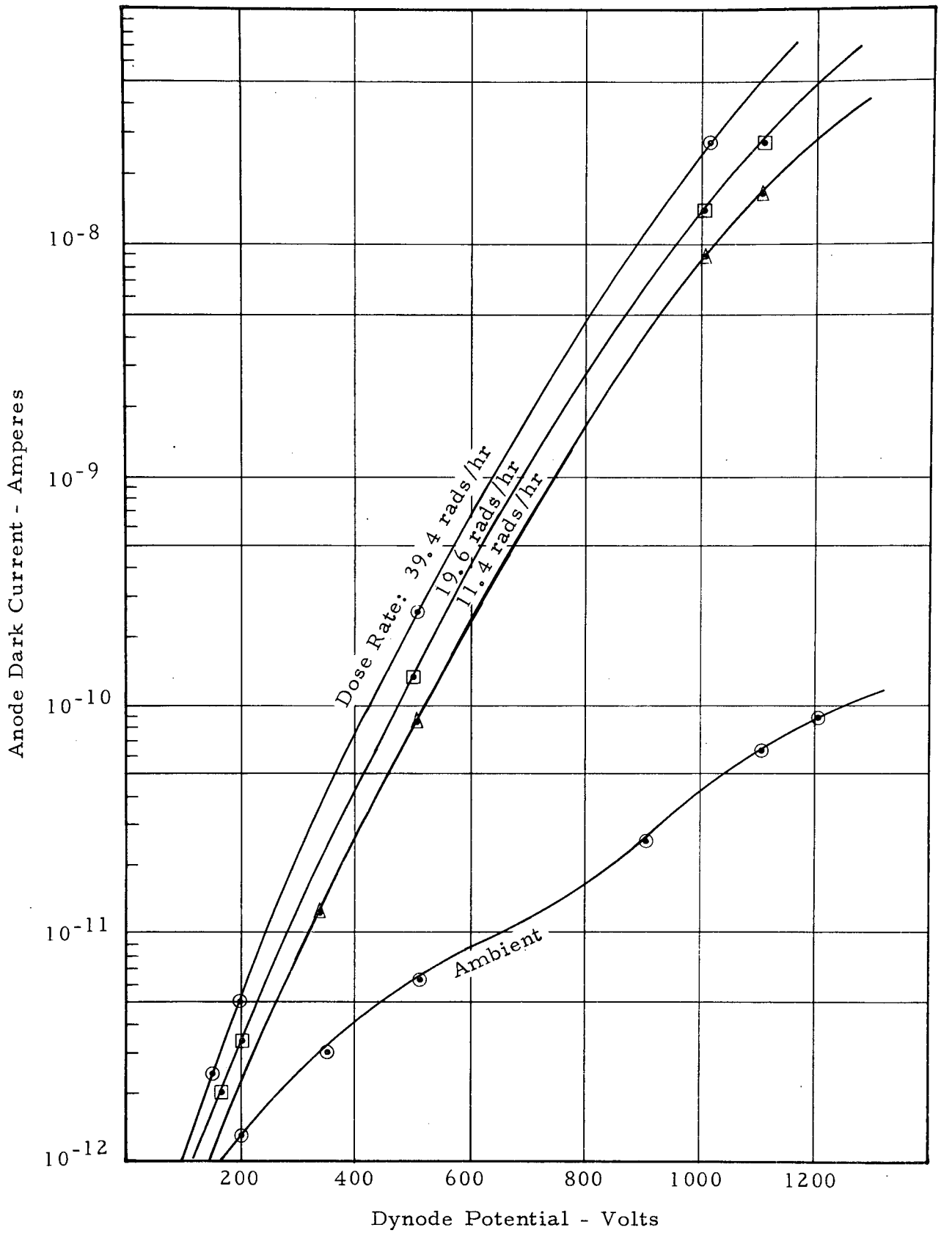

Figure 6-10. GaAs PMT 31025J Dark Current as a Function of Dynode Voltage for Various Radiation Dose Rates (^{60}Co Source)

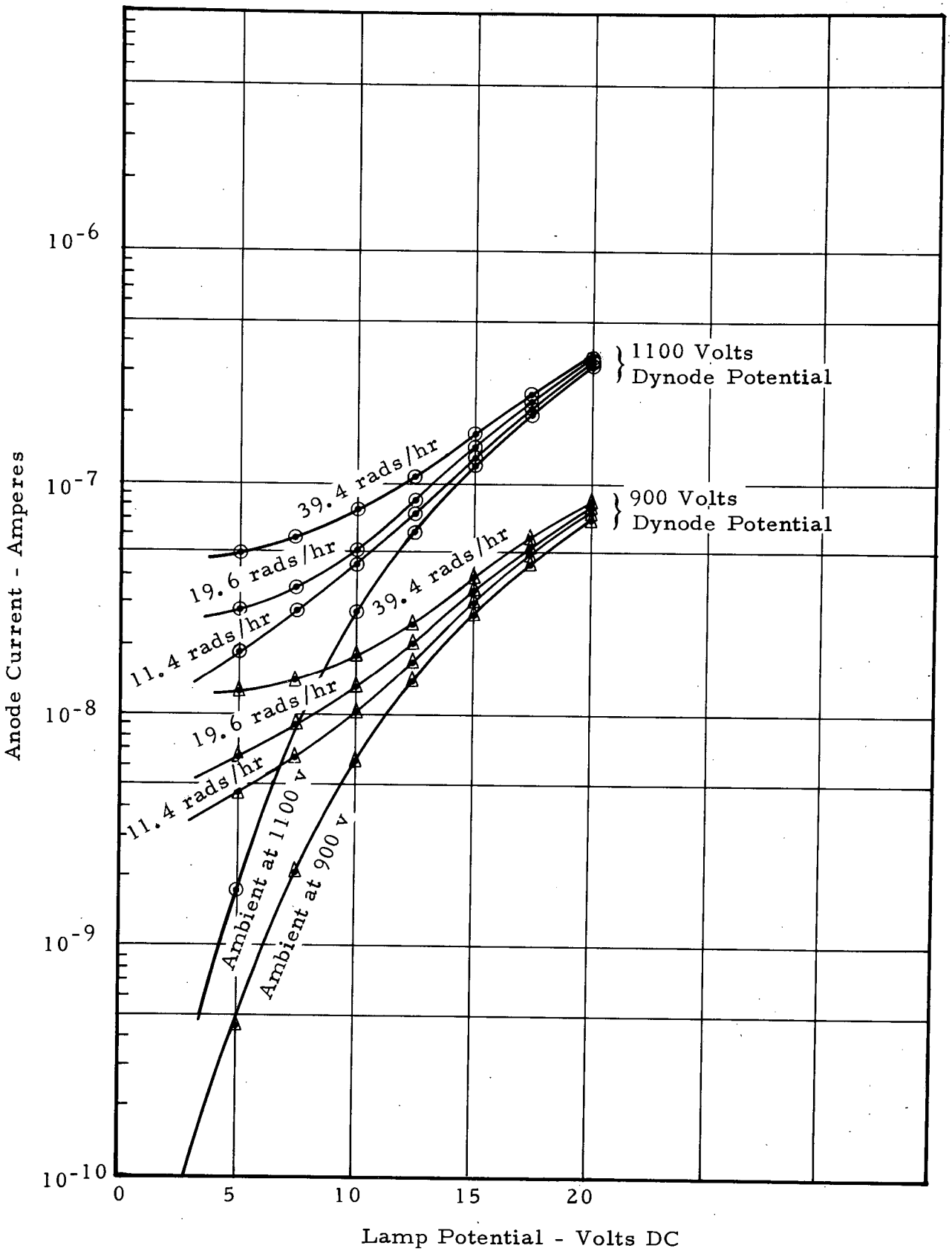

Figure 6-11. GaAs PMT 31025J Anode Current as a Function of Illumination at Various Radiation Dose Rates (^{60}Co Source)

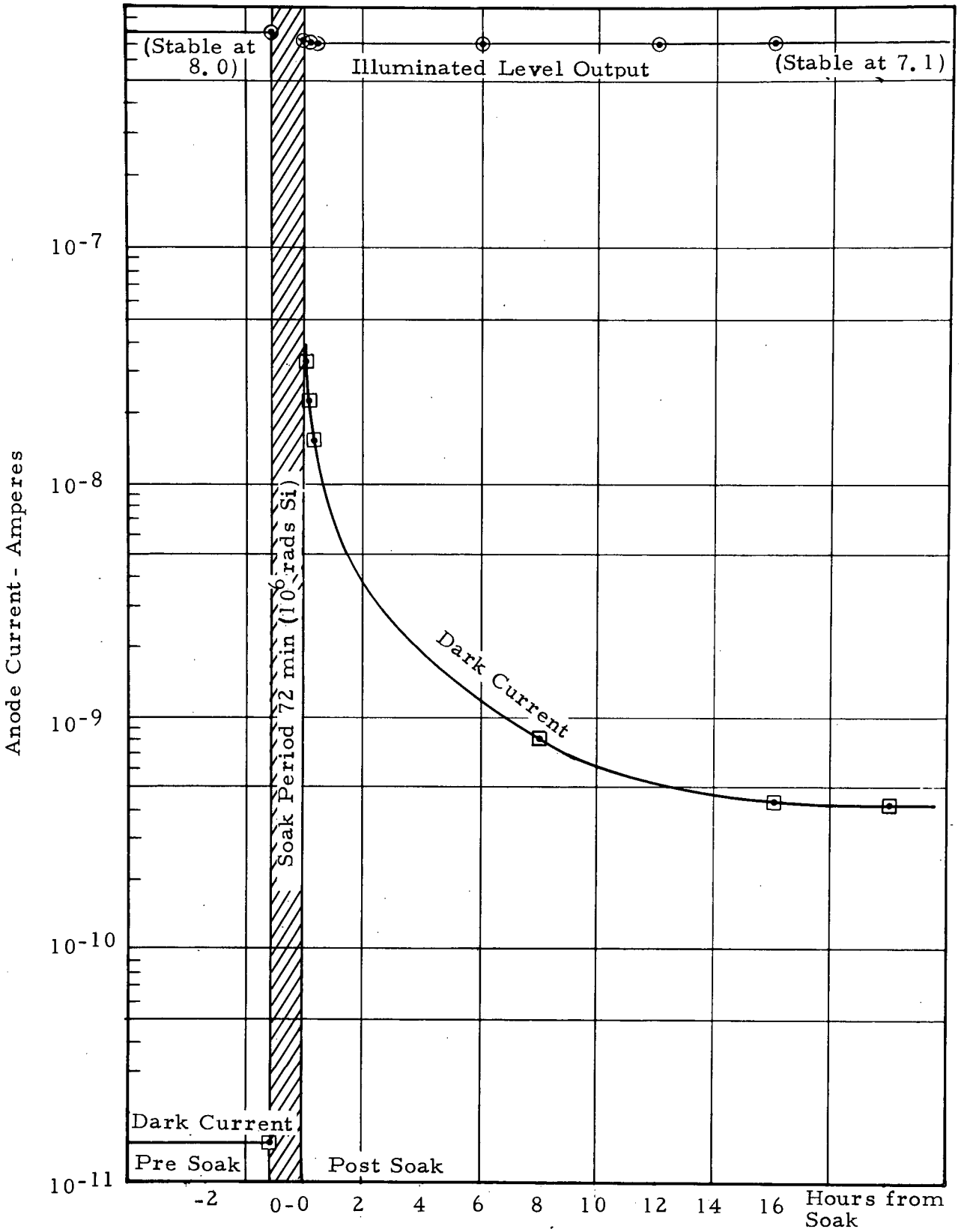

Figure 6-12. GaAs PMT C31025J Output Current as a Function of Time Before and After Exposure to 10^6 rads (Dark Current and Illuminated)

Section 7
SUMMARY

The optical design and component study results have been presented for an OPGT photometer-polarimeter capable of meeting the requirements for both planetary and low light level photometry and polarimetry. A discussion of the detector options available for use on the OPGT has been given as well as test results obtained with a GaAs photomultiplier. The selection of a GaAs photomultiplier as the detector was necessitated by the combination of the required spectral coverage and the low light level signal-to-noise ratio performance. Primarily, the choice of the RCA C31025J photomultiplier for detailed testing was due to the lack of availability of any competing off-the-shelf GaAs photomultipliers. Secondly, the characteristics of the multiplier section are well known. However, this RCA detector exhibited quite satisfactory characteristics during the testing accomplished during this study.

Although the RCA GaAs photomultiplier performed up to expectation, it is appropriate to discuss here some of the characteristics that a more optimum photomultiplier for OPGT would have. Obviously, it would be desirable to reduce tube size and weight somewhat. The size and location of the photocathode within the tube are probably the most serious defects. The photocathode aspect ratio is 2.5:1 which means that the photocathode area is 2.5 times larger than necessary for the OPGT instrument (assuming the image width just equals the photocathode width). This added area will lead to higher dark signal and dark noise, and greater susceptibility to radiation effects. The location of the photocathode on the opposite side of the tube from the window means that the f/No. of the flux incident on photocathode must be relatively large. This necessitates a larger cathode than would otherwise be necessary with the consequent disadvantages mentioned previously. Finally, the grid wires located near the tube window require that much greater care be exercised in the selection of the radiometric and polarimetric

calibration of the instrument; i. e., for some calibration source/geometry choices the grid wires would affect the calibration result even with Fabrey imaging used in the instrument.

Finally, it is pertinent to point out how the OPGT photometer-polarimeter might be modified to yield a more optimum instrument if planetary measurements alone were required. Obviously, such a change would have some impact on both the optical design and detector selection. The basic optical design for the OPGT would also serve for strictly planetary work. Since the throughput or solid angle-area product can be reduced appreciably and still yield adequate SNRs, the major change would be a simple scaling down of the size of the optics. If this is done, then the use of a calcite Wollaston prism would again be competitive with the MacNeille or thin-film polarizing beam splitter. This follows since the path length in the analyzer (MacNeille or Wollaston) is — to a first approximation — reduced proportionately as either the telescope diameter or field angle is decreased. Thus, radiation effects — darkening, fluorescence and Cerenkov radiation — can be significantly reduced with a smaller, simpler instrument.

For planetary-type measurements the use of solid-state detectors — probably UV enhanced, silicon photodiodes — would probably provide the best compromise between system performance and simplicity. SBRC has used silicon photodiodes in both the photovoltaic and photoconductive modes for radiometric measurement in past space instrumentation. As a result, with the exception of the lack of extensive radiation effects measurements, a significant amount of "knowhow" has been accumulated with this type of detector. A tabular summary of pertinent detector parameters and comments is presented in Table 7-1 for convenience.

Table 7-1. Comparison of Detectors for the OPGT Photometer-Polarimeter

Characteristic	PIN Diode	PMT	Channeltron BX-784	GaAs PMT RCA C31025J
Spectral Range	200 to 1100 nm in one detector. Peaks at 900 nm. Low at blue end.	200 to 900 nm in several units. Various responsivities.	Same as PMTs.	180 to 900 nm in one unit. Flat response.
Stability	Relatively unaffected by time, temperature and light overloads.	Varies with time, temperature and light overload.	Finite life (≈1 coulomb). Varies with temperature and time. Sensitive to overexposure.	Relatively stable with time and overloads.
Response Time	Less than 5 ns.	Can be 5 ns - with secondary time constants common to milliseconds - also delay in dynode spread.	2 to 5 ns.	5 to 10 ns for 31025J tested.
Minimum Detectable Light Level	10^{-13} watt for 1 cm^2; 10^{-14} watt for 20-mil diameter.	Single photons.	Single photons with sharp and well defined pulse resolution.	Single photons.
Power	±6 volts to ±20 volts. Relatively insensitive to variations.	900 to 3 kv. Relatively high power for dynode divider.	900 to 3 kv. Low power.	Same as PMT.
Geometry	Unlimited variety. Single elements, arrays, strips, curved surfaces, etc.	Diverse geometries available - some restrict cathode size or acceptance angle.	Single or multiple channels in one envelope. Cathodes 0.020 to 0.2 inch diameter.	Limited at present - restricts acceptance angle and has large cathode aspect ratio.
Radiation Resistance	No degradation at 10^6 rad (Si) accumulated dose.	10 to 50% degradation at 10^6 rad accumulated dose.	15 to 30% degradation at 10^6 rad accumulated dose.	10 to 12% degradation at 10^6 rad accumulated dose.

REFERENCES

1. S. Pancharatnam, Proc. Indian Acad. Sci. A41, 130, 137 (1955).
2. J. M. Beckers, Appl. Opt. 10, 973 (1971); 11, 681 (1972).
3.* Optical Spectra, April 1972; and Industrial Research, May 1972.
4. K. Serkowski, private communication.
5. P. B. Clapman, M. J. Downs, and R. J. King, Appl. Opt. 8, 1965 (1969).
6. A. F. Turner and P. W. Baumeister, Appl. Opt. 5, 69 (1966).
7. E. L. Danahy, "The Real World of Silicon Photo-Diodes," Electro-Optical Systems Design, May 1970.
8. M. V. Schneider, "Schottky Barrier Photodiodes with Antireflection Coating," Bell Systems Technical Journal, November 1966.
9. P. H. Wendland, "Multiple Reflective Laser Detector Diode," Transactions of the Metallurgical Society of AIME, March 1967.
10. W. Eisenman, "UDT PIN-8LC Test Report," NOLC Publication No. 2245, May 1968.
11. Jupiter Radiation Belt Workshop Reports, 21 July 1971 and 9 August 1971.
12. R. Skavland, "Semiconductor Radiation Threshold Assessment for the Pioneer F/G," TRW Internal Memo 69.4334.6-124.
13. J. Brown, S. Bae, S. Park, "Degradation of Multiplier Phototubes Exposed to Spatial Radiations," for NASA-Langley Research Center, under Contract No. NAS1-7648.

*J. J. Brissot and C. Belin, "Preparation of Artificial Calcite Single Crystals by Solvent Zone Melting," J. Crystal Growth 8, 213 (1971).

Appendix

ALTERNATE AFT-OPTICS SCHEME

SANTA BARBARA RESEARCH CENTER

A Subsidiary of Hughes Aircraft Company

INTERNAL MEMORANDUM

TO: MJS Photometer/ Polarimeter Study **CC:** **DATE:** 1 June 1972

SUBJECT: Alternate Aft-Optics Scheme **FROM:** S. F. Pellicori

---

Three problems remain especially outstanding in the design of a precision, compact, light weight photometer/polarimeter.

1). The change of divergence angle of a birefringent analyzer with wavelength necessitating an oversize photocathode.

2). The lack of achromatism in the relay of the exit pupil to the cathode.

3). The inclined cathode of a side-incident PMT shows large sensitivity differences with orientation, and does not yield a mechanically compact instrument.

In addition, any amelioration of the potential energetic particle radiation sensitivity is desirable.

The following scheme is proposed to satisfy the above problems. (See attached sketch).

The orthogonally polarized beams containing all wavelengths are incident on a conic section mirror (perhaps off-axis). The different wavelengths (different angles of incidence) are incident on reflecting areas whose slopes are appropriate to bring the reflected relays into near coincidence on the cathode. The mirror relays the telescope exit pupil image to the cathode. The use of an end-on PMT allows rotation about its axis to obtain optimum response for one specific polarization direction.

This arrangement has been used in an existing polarimeter which was designed for balloon-borne and ground use (S. F. Pellicori and P. R. Gray, Appl. Opt. 6, 1121 (1967)). That polarimeter, however, used spherical mirrors.

/bdlc

S F. Pellicori

S. F. Pellicori

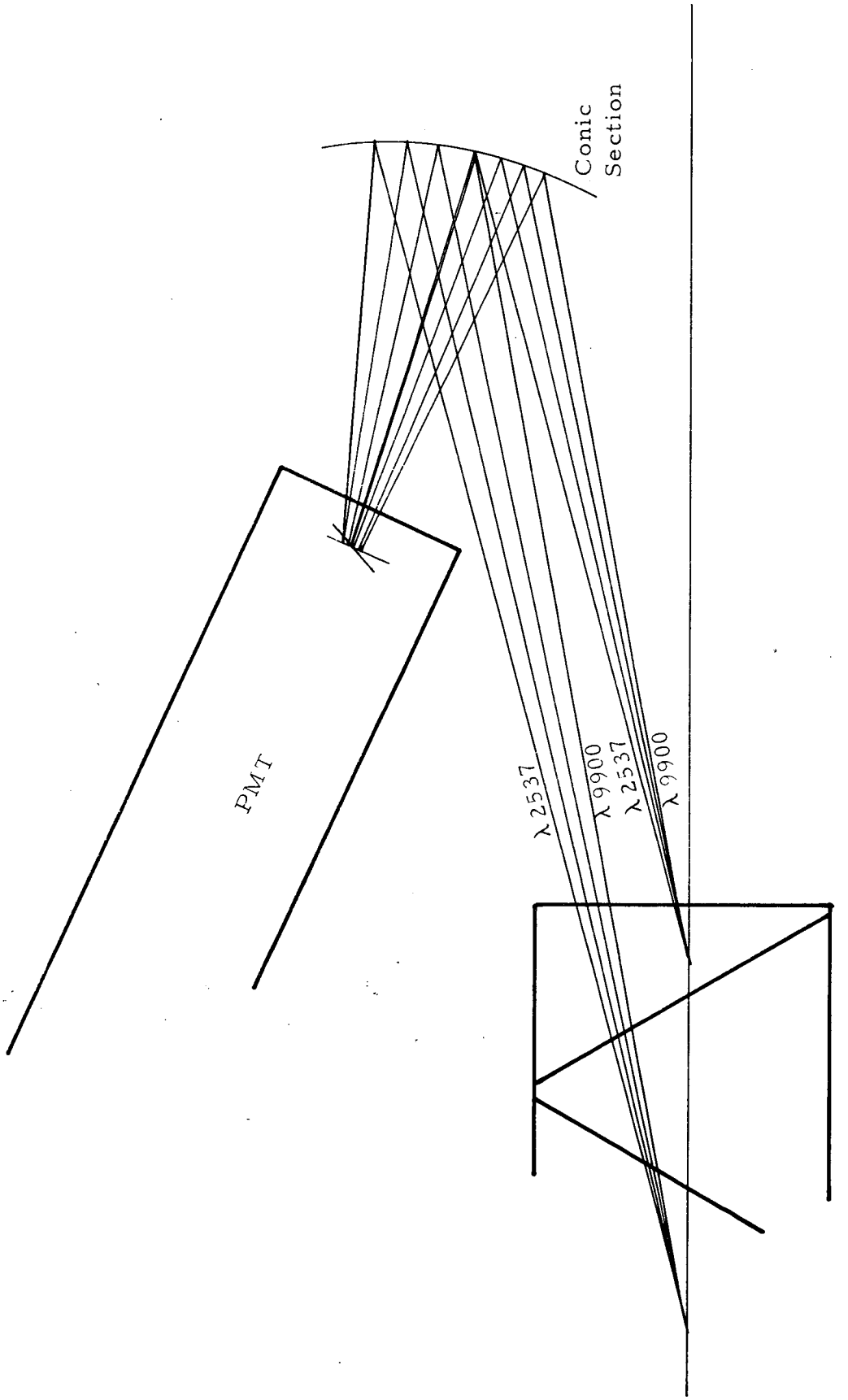

Alternate Aft-Optics Scheme